

Synthesis and thermoelectric properties of some sulfides

A Thesis

submitted to

Indian Institute of Science Education and Research Pune

in partial fulfillment of the requirements for the

BS-MS Dual Degree Programme

by

Prakash Kumar



Indian Institute of Science Education and Research Pune

Dr. Homi Bhabha Road,

Pashan, Pune 411008, INDIA.

April, 2019

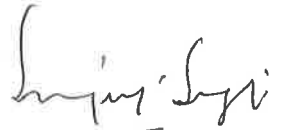
Supervisor: Dr. Surjeet Singh

© Prakash Kumar 2019

All rights reserved

Certificate

This is to certify that this dissertation entitled Synthesis and Thermoelectric properties of some sulfides towards the partial fulfilment of the BS-MS dual degree programme at the Indian Institute of Science Education and Research, Pune represents study/work carried out by Prakash Kumar at Indian Institute of Science Education and Research under the supervision of Dr. Surjeet Singh, Associate Professor, Department of Physics, during the academic year 2018-2019.



Dr. Surjeet Singh

Committee:

Dr. Surjeet Singh

Dr. Prasenjit Ghosh

This thesis is dedicated to my elder brother, Deepak

Declaration

I hereby declare that the matter embodied in the report entitled Synthesis and Thermoelectric properties of some sulfides are the results of the work carried out by me at the Department of Physics, Indian Institute of Science Education and Research, Pune, under the supervision of Dr. Surjeet Singh and the same has not been submitted elsewhere for any other degree.

Prakash Kumar

Prakash Kumar

Acknowledgments

I would like to thank my supervisor, Dr. Surjeet Singh for giving me the opportunity to work on the thermoelectric project in his lab, and for his guidance and encouragement throughout the project. He obviously is a great researcher but also a great human being. He helped me to discover the way a researcher should think about any problem. Overall it was a great learning from him, not only about Physics but also about life.

I would also like to thank all my lab mates, Luminita Ma'am, Saurabh, Prachi, Dibyata, Navita, Bag bhaiya, Anupam, Shivsagar, Rohi, Sanchayeta, Haritha, Nupur and Pragna, without whom this successful journey wouldn't have been possible. Their continuous help academically and morally helped me in overcoming the hiccups in the academic life. The everyday chai pe discussion with these people finally made me addicted to the chai.

I would also like to thank my friends, Akshat, Daman, Jenny, Navita, Vaibhav, Anurag, Dharm, Minal, Sravya and many more without whom I would not have been able to explore this beautiful city, Pune. It was good 5 years with these people with so many ups and downs and someone always by your side to help you and to encourage you.

I would also like to thank the technical staffs of h-cross lab, Mr. Anil, Mr. Nilesh, Mr. Yatthish, Mr. Sudhir and everyone around who helped me in successfully finishing my project.

Finally, I would like to thank my family, my father, mother, brother and sisters and "chota Uttkarsh" who have always been so much supportive and understanding and for all their love they have given me throughout the life. Thank you all!!

Abstract

Materials with promising thermoelectric properties have attracted considerable attention for their use as thermoelectric generators and/or coolers. These devices can be employed to scavenge waste heat from the automobile exhaust, industrial chimneys etc. and transform it back into useful energy. The materials currently in use for such purposes either contain toxic elements or are expensive, thus limiting their commercial application. The sulfides, which are economically viable and environmentally friendly can possibly be used for such application. This project aims to synthesize and study the thermoelectric properties of sulfides of the spinel family which has a general formula, AB_2X_4 . The flexibility allowed by the spinel structure in terms of doping at 'A' and 'B' site, provides scope for fine tuning of the thermoelectric properties.

The samples studied in this project were Cu_2SnS_3 , $CuCo_2S_4$ and $CuZr_2S_4$. Cu_2SnS_3 is not a good thermoelectric material as such; but, doping with Zn or Co or In at the Sn site has helped in enormously increasing the figure of merit, ZT. In cobalt doped sample of Cu_2SnS_3 , the ZT increased from 0.04 to 0.85 by increasing the electrical conductivity by two orders of magnitude. The other compounds, $CuCo_2S_4$ and $CuZr_2S_4$ has been studied previously only for it's use as a low temperature usable material. The high temperature thermoelectric study of these samples and the off-stoichiometric samples would give insights into the use of sulfides as a potential thermoelectric material.

The off-stoichiometric compounds of $CuCo_2S_4$, $Cu_{1-x}Co_{2+x}S_4$ with $x=0, 0.05, 0.1, 0.15, 0.2, 0.5, 0.75$ and 1 were synthesized by the solid state synthesis method. The structural characterization and composition analysis was done using x-ray diffraction and FESEM analysis. The thermal stability, decomposition behavior, composition, phase transitions, melting processes were analyzed by doing the TGA-DSC measurement on the samples using the STA 449 F1 instrument by Netzsch. After this, the thermoelectric properties were measured. The thermal diffusivity, required to calculate thermal conductivity was measured using LFA 1000 apparatus and electrical conductivity and Seebeck coefficient were measured using the LSR-3 Seebeck instrument from Linseis. These properties are mentioned and the behavior of these properties are explained in detail in the thesis.

Contents

Abstract	xi
List of Figures	1
1 Introduction	3
2 Experimental techniques	11
2.1 Synthesis	11
2.2 XRD Characterization	13
2.3 LFA measurement:	13
2.4 LSR measurement	16
2.5 TGA-DSC measurement	17
2.6 FESEM Analysis	19
3 Results and discussion	21
3.1 Cu_2SnS_3	21
3.2 $CuCo_2S_4$	27
3.3 $CuZr_2S_4$	38
4 Conclusion	41

List of Figures

1.1	Effect of thermal gradient on charge carriers [2]	3
1.2	Seebeck effect(left) and Peltier Effect(right) [2]	4
1.3	% Efficiency with ZT [4]	4
1.4	Phonon scattering due to grain boundary, nano-precipitates and point defect [9]	6
1.5	Progress in sulfides [2]	7
1.6	Crystal structure of Cu_2SnS_3 at room temperature[10]	8
1.7	Crystal structure of $CuCo_2S_4$	9
1.8	Band diagram and Density of states	10
2.1	Sealed quartz tubes with pellets	12
2.2	LFA instrument schematic diagram	14
2.3	working principle of LFA measurement	15
2.4	LSR measurement setup	16
2.5	Working principle diagram of LSR measurement	16
2.6	DC four terminal method	17
2.7	TGA-DSC apparatus	18

2.8	FESEM schematic diagram	19
3.1	XRD of Cu_2SnS_3	22
3.2	HTXRD of Cu_2SnS_3	22
3.3	Lattice parameters comparison with temperature	23
3.4	TGA-DSC of Cu_2SnS_3	24
3.5	FESEM images of Cu_2SnS_3	25
3.6	Thermal Conductivity vs. Temperature of Cu_2SnS_3	26
3.7	LSR measurement comparison with reported value	27
3.8	XRD plot of $CuCo_2S_4$	28
3.9	XRD of $CuCo_2S_4$ to Co_3S_4 along with the off-stoichiometric samples.	29
3.10	lattice parameter variation with addition of Cobalt	30
3.11	TGA-DSC data of $CuCo_2S_4$	31
3.12	The figures A-C represents the FESEM images of the samples: A1, A2: $CuCo_2S_4$, B1, B2: $Cu_{0.95}Co_{2.05}S_4$, C1, C2: $Cu_{0.9}Co_{2.1}S_4$,	32
3.13	The figures D-F represents the FESEM images of the samples: D1, D2: $Cu_{0.85}Co_{2.15}S_4$, E1, E2: $Cu_{0.8}Co_{2.2}S_4$, F1, F2: $Cu_{0.5}Co_{2.5}S_4$	33
3.14	The figures G-H represents the FESEM images of the samples: G1, G2: $Cu_{0.25}Co_{2.75}S_4$, H1, H2: Co_3S_4	34
3.15	EDS Analysis of compounds	35
3.16	Thermal Conductivity data of $CuCo_2S_4$ and the off-stoichiometric samples	36
3.17	Density of samples for LFA	36
3.18	LSR measurements for $CuCo_2S_4$ and the off-stoichiometric samples	37

3.19 XRD of $CuZr_2S_4$	39
3.20 XRD of $CuCoZrS_4$	39
3.21 FESEM images, $CuZr_2S_4$	40

Chapter 1

Introduction

The statistical results show that more than half of the energy produced in the world is wasted in the form of heat. Thermoelectricity is direct conversion of heat into electricity and vice versa. Thus, high performance thermoelectric materials have grown attention of governments and research institutes. In 1823, Thomas Johann Seebeck observed that, if two dissimilar metals are joined together and held at different temperatures (T and $T+\Delta T$), a voltage difference ΔV is induced which is proportional to the temperature difference, ΔT . The ratio, $(\Delta V/\Delta T)$ is known as the Seebeck coefficient (S) or the thermopower of the material. This effect is known as the Seebeck effect which is explained using figure. 1.1[2]

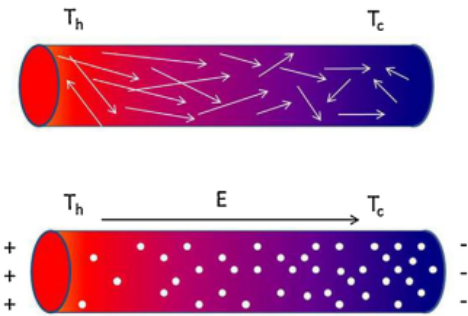


Figure 1.1: Effect of thermal gradient on charge carriers [2]

Here, T_h is the temperature of the hot end and T_c is that of the colder end. Due to the thermal gradient, the charge carriers diffuse from the hot end to the colder resulting in one type of charge carrier getting accumulated at one end, inducing an electric field and thus a voltage difference is created.

There are two types of thermoelectric materials: n-and p-type, which is governed by the majority carriers being electrons and holes, respectively. A thermoelectric device is composed of both n-and p-type materials (known as legs) which are connected thermally in parallel and electrically in series. Thus, the

thermoelectric effect can be used for industrial application using two models as shown in figure 1.2[2]

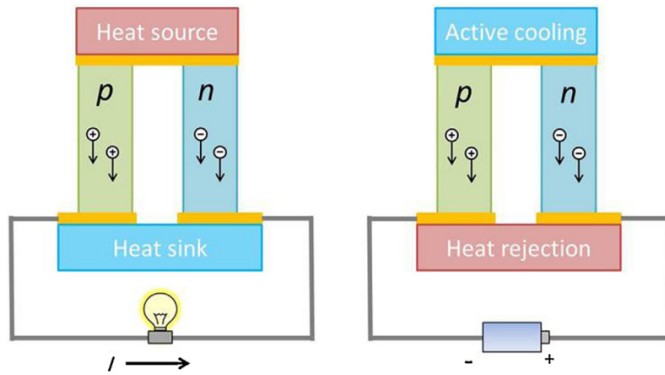


Figure 1.2: Seebeck effect(left) and Peltier Effect(right) [2]

In the first model, Seebeck effect is used for power generation while in the second model, Peltier effect is used for cooling. Peltier effect is just the opposite of the Seebeck effect. In Seebeck effect, the applied thermal gradient drives the charge carriers (holes/ electrons) to move from the hot end to the colder end resulting in a current flow through the circuit while in the Peltier effect, an applied voltage difference across the thermoelectric couple creates the temperature gradient. This happens because the electrical potential applied, induces the charge carriers to maintain the electrical equilibrium by absorbing thermal energy at one end and releasing it at the other.

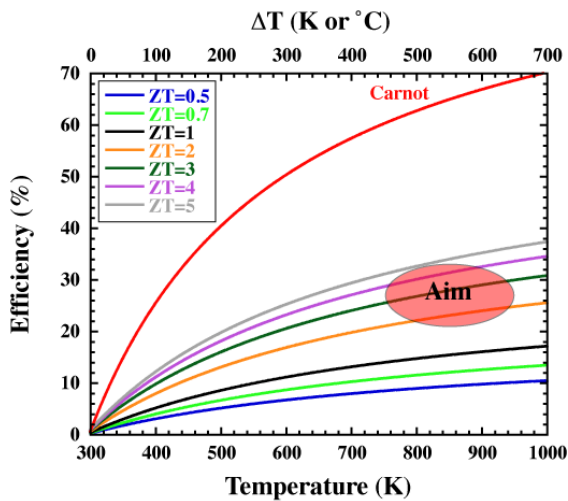


Figure 1.3: % Efficiency with ZT [4]

tion is given by:

$$\eta_p = \frac{T_h - T_c}{T_h} \left[\frac{\sqrt{1 + ZT_{ave}} - 1}{\sqrt{1 + ZT_{ave}} + T_c/T_h} \right]$$

The performance of a thermoelectric device is determined by the dimensionless figure of merit, ZT of its individual legs (n-and p-type materials). The expression for ZT is given by: $ZT = S^2 \sigma T / \kappa$, where S is the Seebeck coefficient, σ is the electrical conductivity, T is the absolute temperature and κ is the total thermal conductivity of the material. Thus an ideal thermoelectric material should have high values of S and σ and very low value of κ . A lower value of κ would make sure that the voltage difference produced due to the temperature gradient can be maintained. The efficiency, ' η ' of a thermoelectric material used for power genera-

where, T_h and T_c is the temperature of the hot and cold end respectively and T_{ave} is the average of T_h and T_c . Thus for a better efficiency, the ZT_{ave} should be as high as possible, and its evident from the figure 1.3[4].

From figure 1.3, we notice that a material with $ZT > 1$ (black line) gives an efficiency of 15% - 20% when the operating temperature at the hot end of the device is as high as 800 K. So, one aims ZT to be as high as possible, but even a material with $ZT=1$ at higher temperatures is considered to be a good thermoelectric material for application purposes.

Coming back to the figure of merit, $ZT=S^2\sigma T/\kappa$. The term, $S^2\sigma$ is known as the power factor. κ is the total thermal conductivity which consists of lattice (κ_l) and electronic (κ_e) contributions. Thus, $\kappa = \kappa_e + \kappa_l$

To obtain a high ZT value, one would like to have a high value of S and σ and a lower value of κ . But the relations between these 3 quantities conspire against this. The Wiedemann-Franz law gives direct relation between electronic thermal conductivity, κ_e and the electrical conductivity, σ by the relation: $\kappa_e=L\sigma T$ where 'L' is the Lorenz number. Thus an increase in σ , in the numerator of ZT will lead to an increase in the κ in the denominator as well. Again from the Pisarenko relation:

$$S = \frac{8\pi^2 k_B^2}{3eh^2} m_d^* T \left(\frac{\pi}{3n} \right)^{2/3}$$

and,

$$\sigma = ne\mu = \frac{ne^2\tau}{m_b^*}$$

where, k_B is the Boltzmann constant, m_d^* is the density of states effective mass, m_b^* is the band effective mass, h is the Planck constant, n is the carrier concentration, e is the electron charge, μ is the charge mobility and τ is the relaxation time. From this complex relation between the parameters, one can see that the tuning of carrier concentration alone cannot enhance ZT . Now, $S \propto m_d^*$ while, $\sigma \propto 1/m_b^*$ and the relation between the two effective masses are given as: $m_d^* = N_v^{2/3} m_b^*$. Thus, increasing Seebeck by increasing m_d^* would lead to increase in m_b^* as well and thus a decrease in σ . Hence, to increase the Seebeck coefficient one needs to decouple m_d^* and m_b^* by controlling the valley degeneracy, N_v .

Now, the parameter which is independent of the carrier concentration is the lattice thermal

conductivity, κ_{lat} and reducing it can thus help to reduce total thermal conductivity. κ_{lat} is given as:

$$\kappa_{lat} = \frac{1}{3} C_v v l$$

Since, heat capacity, (C_v) and the phonon velocity (v) are constant, the mean free path (MFP), 'l' of phonons would decide the lattice thermal conductivity. So, if the spatial dimension of the defects is comparable to the MFP, the phonons will get scattered strongly. Most of the heat is carried by the acoustic phonons, which has a spectrum of wavelength and mean free path distribution and thus synergetically contributes to the total thermal conductivity. Hence, various length-scale structures, like, solid-solution point defects, grain boundaries and nano-scale precipitates, as shown in the figure 1.4[9], are the main features taken into consideration while synthesizing the thermoelectric materials with a reduced lattice thermal conductivity.

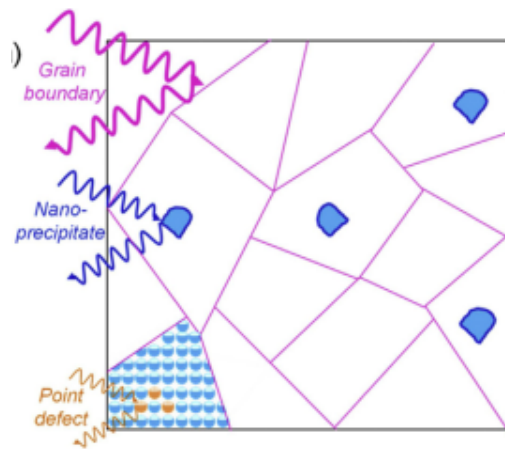


Figure 1.4: Phonon scattering due to grain boundary, nano-precipitates and point defect [9]

The methods like doping or alloying can be used to form point defects. The mass difference leading to mass fluctuations and the size and the interatomic coupling force differences leading to strain field fluctuations between the parent lattice and point defects leads to the enhanced phonon scattering and thus reducing the lattice thermal conductivity. Also, doping in the TE materials optimizes the electrical transport properties by tuning charge carrier concentration.

The thermoelectric device is silent, as it does not involve moving parts, and can, therefore, be employed with relative ease in places like automobile exhaust and industrial chimneys to scavenge the waste heat and transform it back into useful energy.

However, till date these devices have found applications in niche and remote areas only, including their use as power generators in space satellites and TE coolers in many sophisticated research equipment. In general a TE device with $ZT > 1$ is considered suitable for commercial application. So, compounds like Bi_2Te_3 with high ZT near room temperature; and, in the intermediate temperature range, $PbTe$, are already being used in power generation applications. But they both contain toxic elements that are hazardous to health. Apart from these two materials there are a few other materials but they also contain either high cost elements or have highly toxic elements which

has limited their large-scale application. For this reason, currently there is a significant interest in discovering or developing new materials consisting of elements that are earth abundant (hence economically viable) and non-toxic. In this regard, the materials of sulfide family have recently gathered significant attention.

Though there is no theoretical upper limit on ZT, and the maximum value reported so far for the bulk materials is less than 3. For sulfides ZT is even lower, highest value less than 1.5. Some of the sulfides with a reasonably high ZT include Bi_2S_3 [1], $Cu_{2-x}S$ [11] and Ag_2S [7]. However, sulfur being one of the most abundant, environmental friendly and non-toxic elements, sulfides with a value of ZT above 1 are expected to be considered importance. These advantages of sulfides suggest that metal sulfides should be promising TE materials, but the challenges like the low melting point of sulfur, volatility at high temperatures, light atomic weights and intrinsically too low or too high carrier concentrations greatly limit the metal sulfides to have very high efficiency in energy conversion. But there has been continuous search for sulfides as a good thermoelectric material. From Figure 1.5, it is evident that Sulfides can also achieve ZT more than 1 for compounds like $Cu_{1.97}S$ and $Cu_{1.98}S$. Thus, with thermoelectrics being an active area of research, sulfides can be proved to be highly useful in scavenging useful energy from the waste heat with advantages of being environmental friendly and cheaper as well.

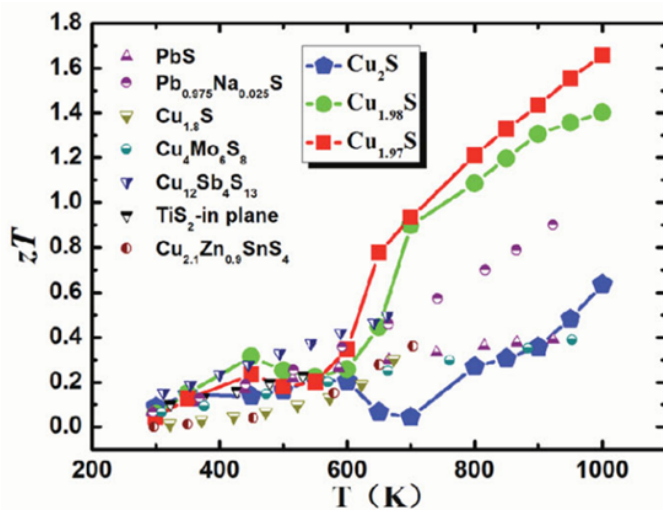


Figure 1.5: Progress in sulfides [2]

Zhao et al. by Co-doping at the Sn-site[J Mat. Chem. A (2017)][10]. The other material that we investigated here is $CuCo_2S_4$, whose thermoelectric properties have not been investigated till now.

In this project, our aim was to develop sulfur based TE materials with high thermoelectric performance, and not involving toxic and expensive constituents. The materials investigated was Cu_2SnS_3 , where the band structure calculation suggests that the valence band consists of Cu 3d orbitals and S 3p orbitals, which leads to a Cu-S conductive network. Recently a moderately high ZT of 0.58 (at 723 K) was reported by Yawei Shen et al.[5] in Zn-doped Cu_2SnS_3 , and upto 0.9 by

As an eco-friendly sulfide TE material, Cu_2SnS_3 has attracted a significant attention. The phonon glass electron crystal characteristic of the sample gives scope to the researchers to enhance its thermoelectric properties by various approaches. The "Phonon glass electron crystal" approach states that for a good thermoelectric material, the material should behave as a glass for the phonons and as a crystal for the electrons. Glass being amorphous scatters phonons, which are responsible for carrying the heat through the sample. Since, most of the phonons would get scattered, very small amount of heat will be conducted through the sample and thus such materials will have lower lattice thermal conductivity, κ_l and thus lower total thermal conductivity, ' κ ' as well. The crystal nature of the material will allow the electrons to flow smoothly and thus would help in achieving high electrical conductivity, ' σ '.

Cu_2SnS_3 can adopt several structures like cubic at high temperatures along with monoclinic, tetragonal and triclinic phases as well at low temperatures[8]. The monoclinic structure, at room temperature is shown in the figure 1.6[10]. The compound Cu_2SnS_3 also transforms structure upon doping. It goes from the monoclinic structure for the pristine sample to cubic upon doping 10% Co at Sn site and further doping by 20% Co transforms it into a tetragonal structure[10]. In these two structures, cubic and tetragonal, there is order-to-disorder atomic arrangement, which plays a significant role in phonon scattering and thus reducing the lattice thermal conductivity to as low as 0.9 W/m/K at room temperature; and 0.33 W/m/K, at 723 K(450 °C). Thus, for 20% Cobalt doped sample, one can achieve a power factor as high as $9.4 \mu\text{W}/\text{cm}/\text{K}^2$ at 723 K and thus also a high ZT of 0.85 at this temperature.

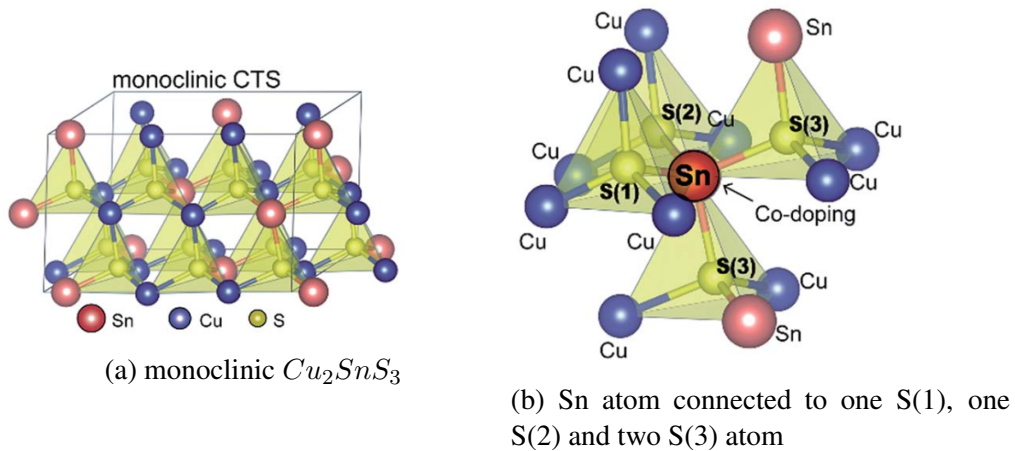


Figure 1.6: Crystal structure of Cu_2SnS_3 at room temperature[10]

The pristine material, Cu_2SnS_3 also has a low thermal conductivity of 1 W/m/K to 2.5 W/m/K.

Also it has low value of electrical conductivity of 2 S/cm to 7 S/cm. But it is the high value of Seebeck coefficient of 270 $\mu\text{V/K}$ to 450 $\mu\text{V/K}$ from room temperature to 450 $^\circ\text{C}$ which make the compound interesting to study. So, researchers in recent times have tried to increase the value of electrical conductivity by doping in this sample.

In one such attempt, Yawei Shen et. al.[5] could achieve a ZT of 0.58 at 723 K by doping Zinc at the place of Tin in Cu_2SnS_3 . Also, Huiwen Zhao et. al.[10] could achieve a ZT of 0.85 at 723 K by doping Cobalt at the Tin site in Cu_2SnS_3 .

CuCo_2S_4 , mineral carrolite belongs to the group of spinels, with general formula AB_2X_4 , where X anions are typically Chalcogens like oxygen and Sulfur. The cations A and B occupy the octahedral and tetrahedral sites in the lattice. The thiospinel, CuCo_2S_4 crystallizes in the cubic structure (space group Fd-3m) with Copper at the tetrahedral site and Cobalt at the octahedral site surrounded by Sulfur atoms as shown in the figure 1.7[6].

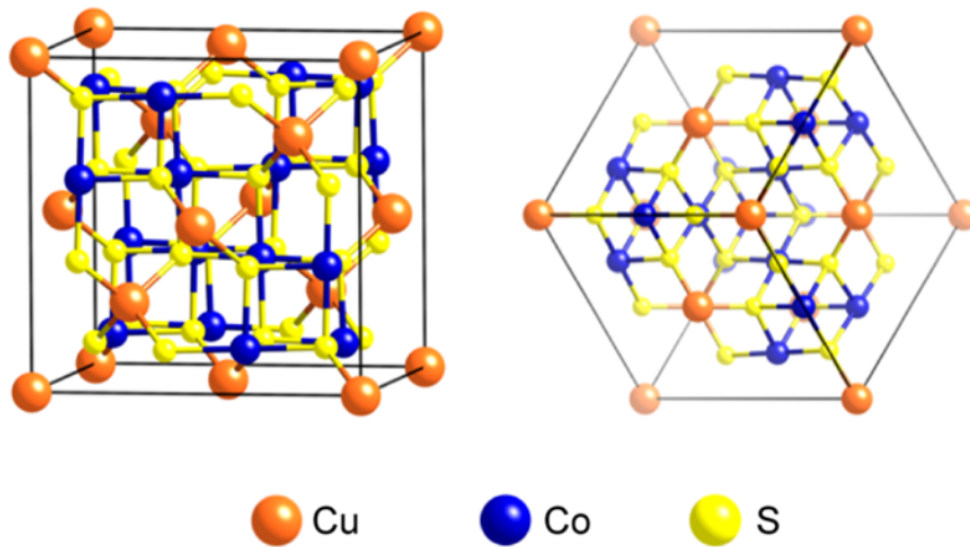
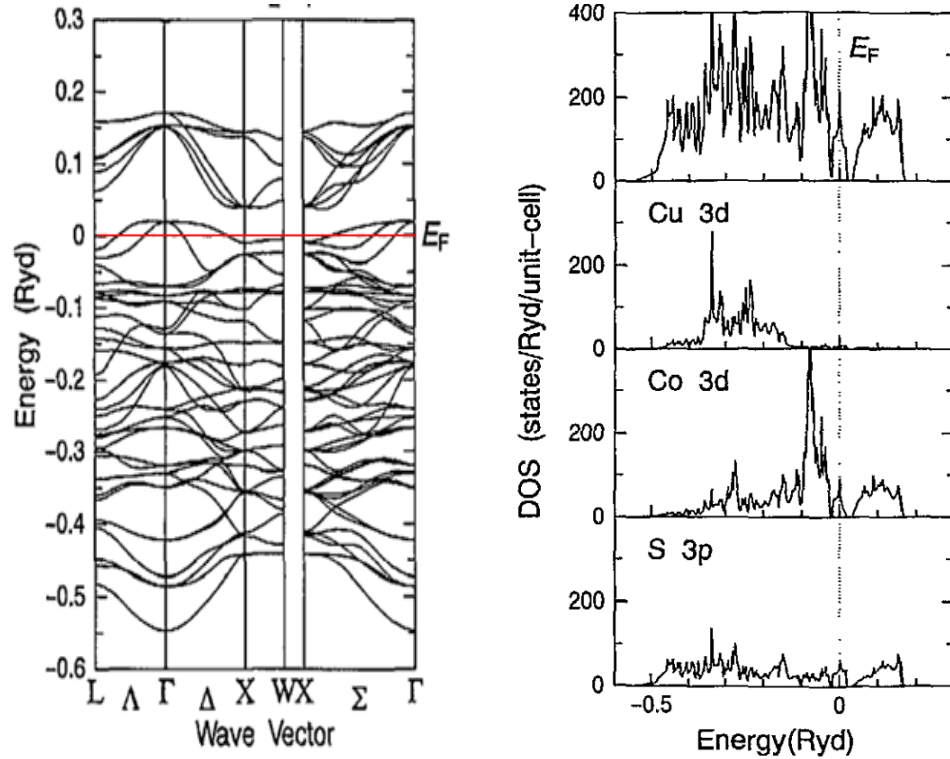


Figure 1.7: Crystal structure of CuCo_2S_4
[6]

This group of compounds have been reported to show interesting magnetic and electrical properties at low temperatures. CuCo_2S_4 shows an antiferromagnetic order below the Neel temperature $T_N = 18\text{K}$. The flexibility of the spinels family of compounds allows one to play with the A and B atoms in terms of doping to fine tune the thermoelectric properties of these spinel compounds. However, CuCo_2S_4 has already been reported to show a metal like behavior at room temperature,

and thus high value of electrical conductivity. The Copper atoms are present here as Cu^{2+} , cobalt atoms as Co^{3+} while the Sulfur anions as S^{2-} . The off stoichiometry at the copper site or the cobalt site is expected to introduce defects in the lattice causing enhanced scattering of phonons and thus leading to decrease of the thermal conductivity. This can also change the mobility of the charge carriers which can greatly affect the electrical transport.



(a) Energy band dispersion of $CuCo_2S_4$ (b) Total and partial DOS of $CuCo_2S_4$

Figure 1.8: Band diagram and Density of states

From an article by T Oda et. al. in 1995 in the J. Phys.: Condens. Matter [3], they calculated that the Fermi level, E_f of $CuCo_2S_4$ lies below the top of the valence bands as shown in figure 1.8 (a) and thus there exists unoccupied bands. Among the thiospinels $CuRh_2S_4$, $CuIr_2S_4$ and $CuCo_2S_4$, the total density of states at the Fermi level is largest for $CuCo_2S_4$ and in all of the three spinels, the contribution to the total DOS is least from Cu-3d while the contribution is quite comparable for Co-3d and S-3p orbitals as shown in figure 1.8 (b). Therefore, the contributions from the S-3p and Co-3d orbitals play an important role here in studying the transport properties since they are dependent on the electronic states near the Fermi level.

Chapter 2

Experimental techniques

2.1 Synthesis

Arc melting: This is used for melting metals to form alloys. In this method, an arc is generated by passing current of 15A through the Tungsten electrode and then creating an electric discharge by touching the tip of the electrode with the Zirconium pieces kept inside. The Zirconium here is used also to consume any oxygen present in the surrounding and hence is first melted using the arc produced. The chamber is evacuated 5 times and filled with Argon to remove any other gas present. Argon being an inert gas doesn't react with the molten metal. The melted sample is turned over and remelted to ensure homogeneity of the sample.

Solid state reaction: The sample precursors after grinding was pelletized by cold pressing it for around 6 minutes in a circular die using a KBr press. The amount of pressure applied depends on the dimension of the pellet being made, for e.g. 3 tons of pressure for 8mm pellet. The pellets were then quickly transferred in a long (approx.30cm) quartz tube with inner diameter 10 mm and sealed from one end. The tube is then sealed by creating a dynamic vacuum of around 10×10^{-4} torr. The sealed tubes as shown in the figure 2.1 are then kept inside the furnace for the desired heat treatment. The same process is repeated until one gets the desired compound.

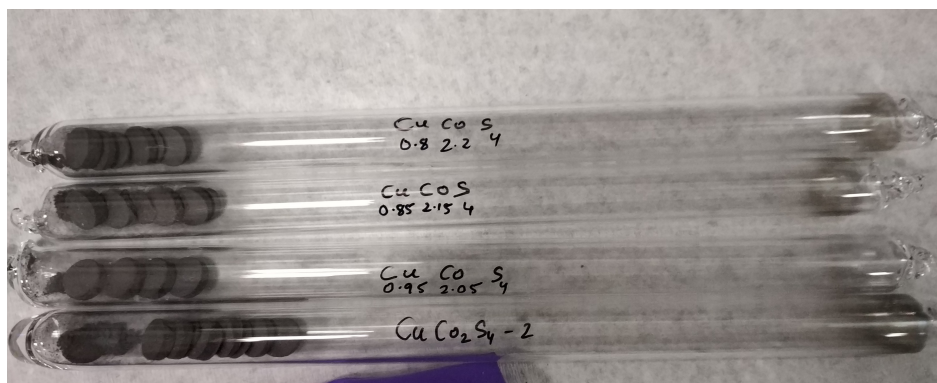


Figure 2.1: Sealed quartz tubes with pellets

The samples synthesized were:

1. Cu_2SnS_3 : Since we had pieces of Cu and Sn and not their powder, first of all an ingot of Cu_2Sn was formed using arc melting. This ingot was broken into pieces and then grounded to mix it thoroughly with sulfur. The powders were then pelletized and sintered at $700^\circ C$.

$CuCo_2S_4$ and off stoichiometric samples: The powders of Cu, Co and S were grounded, pelletized and then sintered.

2. The first sample of $CuCo_2S_4$ was sintered twice at $700^\circ C$ while the second sample was sintered thrice at $500^\circ C$ for 24 hours.

3. $Cu_{1.1}Co_{1.9}S_4$ and $Cu_{0.9}Co_{2.1}S_4$: The pellets were sintered first at $600^\circ C$ and then at $500^\circ C$ for 24 hours each.

4. $Cu_{1-x}Co_{2+x}S_4$, $x=0, 0.05, 0.15, 0.2$: These samples were sintered 3 times at $500^\circ C$ for 24 hours.

5. $Cu_{0.25}Co_{2.75}S_4$ and $Cu_{0.5}Co_{2.5}S_4$: The pellets were sintered at $500^\circ C$ for 24 hours thrice and then at $600^\circ C$ for 24 hours for the 4th sintering.

6. Co_3S_4 sample was sintered once at $500^\circ C$ for 48 hours.

7. $CuZr_2S_4$ and $CuCoZrS_4$: The precursors were grounded inside the glove box in the Argon atmosphere to avoid any reaction of Zirconium in air. The precursors were then transferred in an alumina crucible inside a quartz ampoule. The precursors were heated slowly @ $30^\circ C/hr.$ to 350

°C and then even slower @ 4°C/hr. to 750 °C and was kept at 750 °C for one week and then cooled again to room temperature @ 30°C/hr.

2.2 XRD Characterization

Powder X-Ray Diffraction is a very commonly used technique to analyse the structure of crystalline materials. The periodic arrangement of atoms in a crystal can be visualised in the form of atomic planes. These planes behaves like 3 dimensional diffraction grating when X-ray of wavelength comparable to the interplanar distance is incident. The X-ray gets diffracted and its intensity can be detected depending on the constructive or destructive interference which is governed by the following condition:

If, $n\lambda=2d\sin\theta$, then only x-rays interfere constructively

Where n is the order of diffraction, λ is the wavelength of X-rays used, d is the inter-planar spacing and θ is the angle of the incident x-ray beam with the plane of the sample.

The X-ray diffraction analysis was done on the powder sample on a glass slide by sprinkling powder on to the oil to stick the sample and also to keep the height of the sample constant throughout. Since, both glass and oil are amorphous, they donot contribute to the XRD spectrum. The Bruker D8 advance setup was used for the x-ray diffraction measurements which uses $\text{Cu } K\alpha$ radiation of wavelength 1.5406 Å. By matching the peaks with the JCPDS data available in the software, we could confirm the purity of the phase or if there were any additional peaks present due to some other impurity phase. Silicon was mixed with the sample powder to find any shift in the peaks because of lattice expansion or contraction for the off-stoichiometric samples. This was also used for finding the lattice parameters of the crystals using the Unit cell software by taking silicon peaks as the reference.

2.3 LFA measurement:

The LFA measurements were done on the 6mm or 8mm circular pellets on the Linseis LFA 1000 setup. The measurements were done till high temperatures upto 450 °C. The schematic of the setup

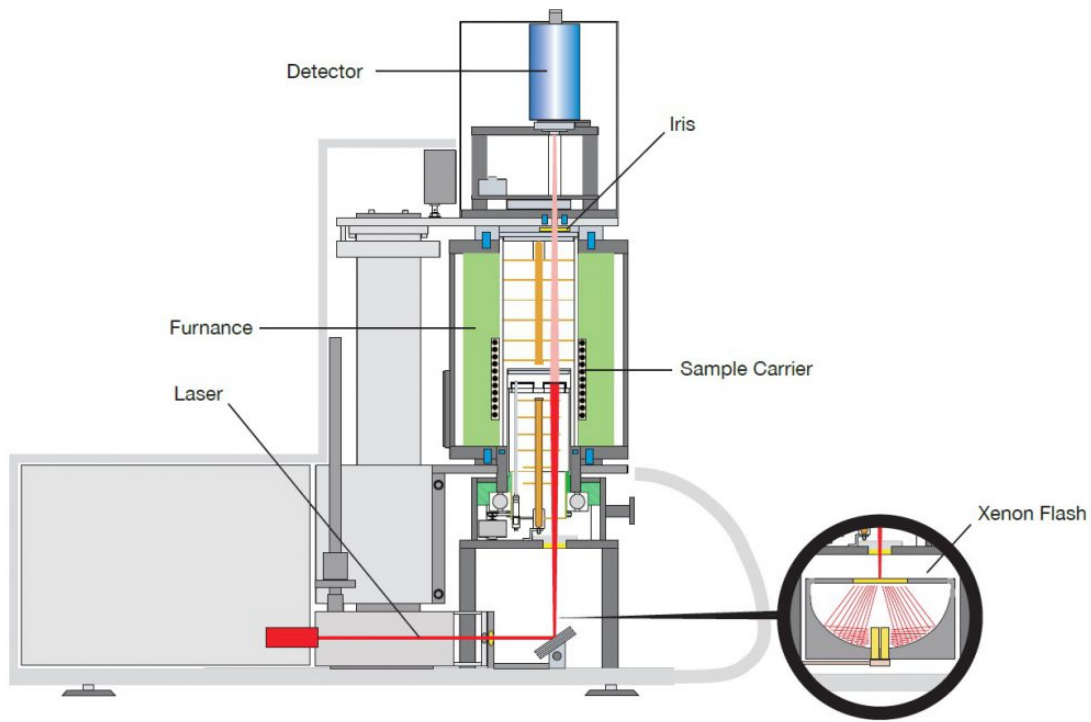


Figure 2.2: LFA instrument schematic diagram

is shown in figure 2.2.

The principle of the measurement is shown in the figure 2.3. The laser comes out horizontally and then it is directed vertically on to the sample. The temperature of the sample is measured using a thermocouple which is present at the center of the sample holder and is at the same height as that of the sample.

The sample is surrounded by a furnace which heats the sample and its surroundings to a specified temperature. A programmable energy pulse irradiate the back side of the sample, resulting in a homogeneous temperature rise at the sample surface. The resulting temperature rise of the surface of the sample is measured by a very sensitive high speed IR detector cooled continuously with liquid nitrogen. The thermal diffusivity can be determined from the temperature vs. time data using the formula: $D = 0.13879 \times L^2 / t_{1/2}$, where 'L' is the thickness of the sample and $t_{1/2}$ is the time required to reach the $\Delta T_{1/2}$. $\Delta T_{1/2}$ is the half of the maximum temperature rise, ΔT_{max} . Therefore, one should set the measurement time such that the saturation temperature is reached within that time. The software then fits the temperature vs. time data using the various models like

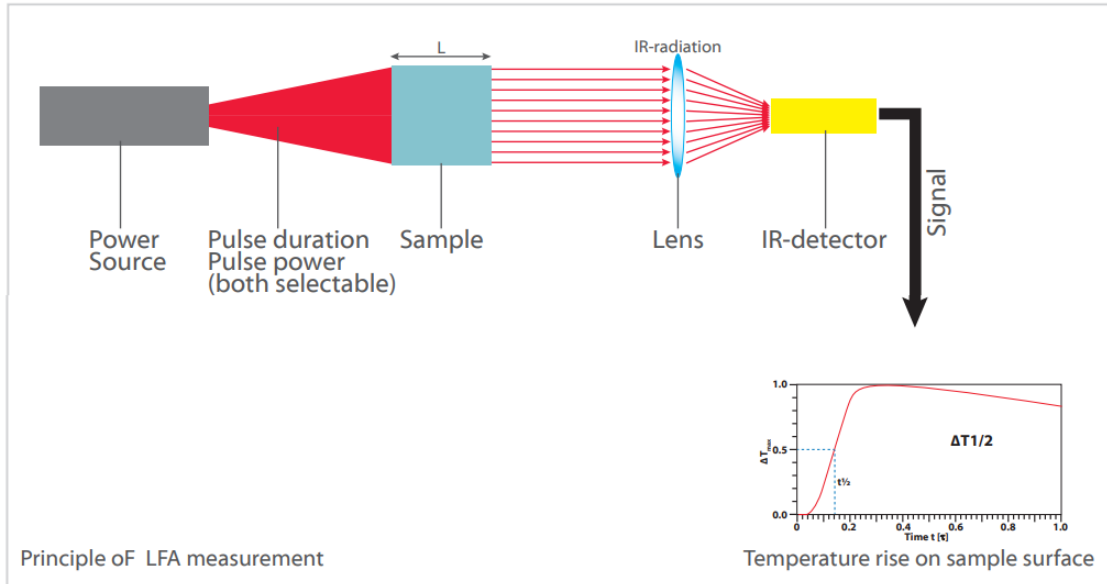


Figure 2.3: working principle of LFA measurement

combined, heat loss, radiation, adiabatic model etc. The percentage of fit also decides the quality of the data and hence, for all the measurements, the fit catalogue was set to 96%. So, all the data with fit lesser than 96% gets discarded as bad data points and are not used for calculations.

After obtaining the thermal diffusivity (D), one can calculate the thermal conductivity (κ) as a function of the temperature using the formula: $\kappa(T) = D(T) \times C_p(T) \times \rho(T)$ where, $C_p(T)$ is the specific heat capacity of the sample as a function of temperature and $\rho(T)$ is the density of the sample as a function of temperature. Here, we assume density, ρ of the sample to be constant and was measured using the mass of the sample and its dimensions before loading the sample for measurement. The specific heat capacity, C_p is approximated by the Dulong-petit law and is assumed to be constant as well throughout the temperature range.

As can be seen from the formula that the thermal conductivity is dependent on the density, a lower density sample would give low thermal conductivity value and thus a wrong and over estimate of the figure of merit (ZT) since, ' κ ' comes in the denominator of the formula for calculation of ZT . All the measurements were done in vacuum and at each temperature, 3 measurements were done and then later averaged to give the thermal conductivity at that particular temperature.

2.4 LSR measurement



Figure 2.4: LSR measurement setup

The Seebeck coefficient and the resistivity of the sample was measured using LSR-3 Seebeck apparatus. The sample were rod shaped with length around 7mm-8mm and all the measurements were done in Helium atmosphere till 450 °C. The schematic of the instrument is shown in the figure 2.4.

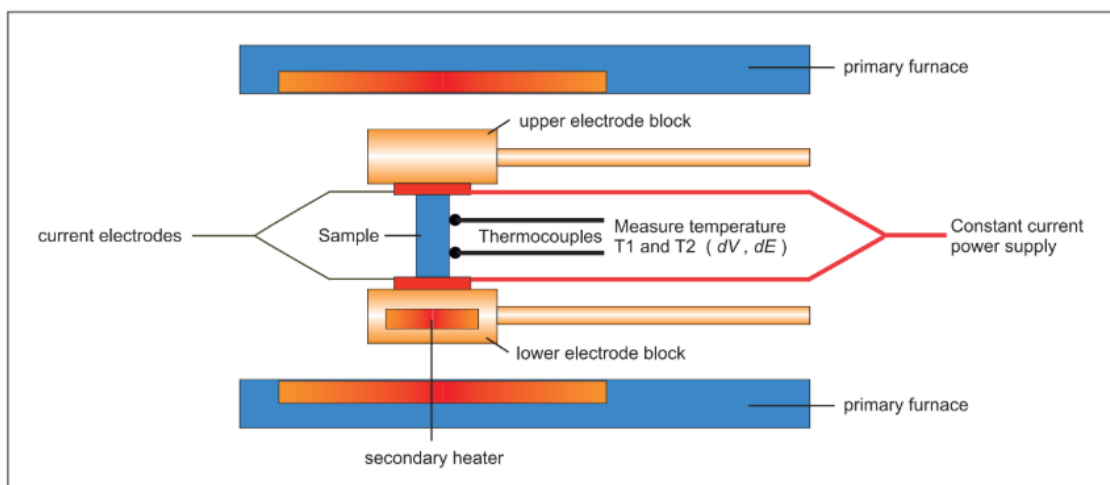


Figure 2.5: Working principle diagram of LSR measurement

As shown in the figure 2.5, the sample is placed vertically between the two electrodes. The lower electrode block contains a heater known as secondary heater, surrounded by a furnace which heats the sample to a specified temperature. At this temperature, the secondary heater creates a set temperature gradient. The two contacting thermocouples then measure the temperature gradient T_1 and T_2 . A unique thermocouple contact mechanism permits highest accuracy measurements of the electromotive force dE at one wire of each of the two thermocouples.

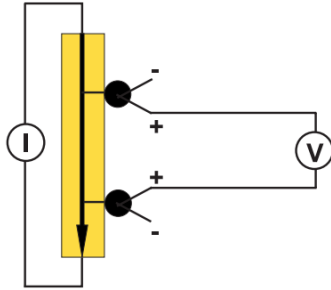


Figure 2.6: DC four terminal method

The dc four-terminal method as shown in figure 2.6 is used to measure the electrical resistance by applying a constant current (I) at both ends of the sample and measuring the change in voltage dV between one wires at each of the two thermocouple. The software, TAWIN of the LSR-3 system records the resistivity (ρ) and the relative Seebeck coefficient data of the sample. The Relative Seebeck coefficient comes because of the contribution from the platinum of the probes and one needs to get rid of it to get the Absolute Seebeck coefficient (S) of the sample which is done using the software. The images of LFA and LSR instrument were taken from the website of Linseis.

2.5 TGA-DSC measurement

The thermal analysis was done using STA 449 F1 by Netzsch as shown in the figure 2.7. This instrument simultaneously does Thermogravimetry Analysis (TGA) and Differential Scanning Calorimetry (DSC) on the same sample in a single run. The advantages are that the test conditions are perfectly identical for the TGA and DSC signals (same atmosphere, gas flow rate, vapor pressure on the sample, heating rate, thermal contact to the sample crucible and sensor, radiation effect, etc.). Also, sample throughput is improved as more information can be gathered from each run. For doing the TGA-DSC, the carrier contains two crucibles, one of which is used as reference for the measurement.

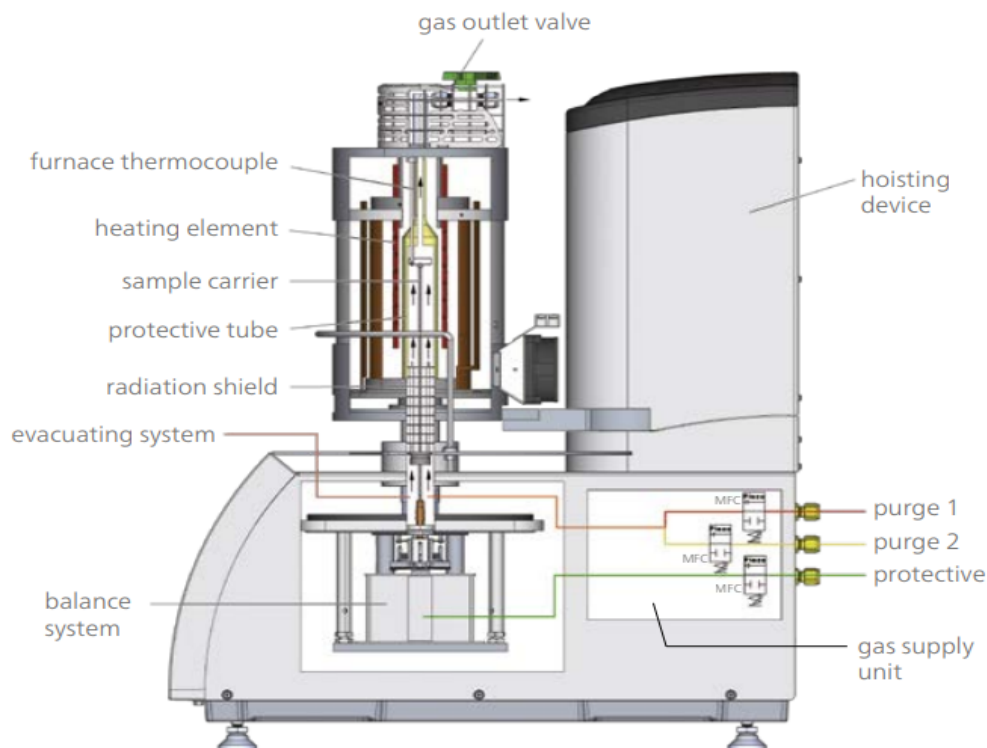


Figure 2.7: TGA-DSC apparatus

First of all the blank run is done with both the crucibles empty. The data of blank run gets subtracted from the sample data. The temperature and the gas flow rate when doing the blank run are kept the same as one will be doing with the sample. The sample is loaded in one of the crucible and for TGA, the balance is tared to zero and after waiting for few minutes to stabilize the balance reading after the gas flow was turned ON, one can start the experiment. The high purity gases used were Nitrogen gas for the balance (Protective gas) while Argon was used for the sample chamber (Purge gas). The mass of the sample taken was around 15mg-20 mg. The instrument is highly sensitive to vibrations and thus care must be taken while doing these measurements. The data was analyzed using the Proteus software. Here, one can easily find out the mass change in weight % or in mg. Also one can analyze, the position of the DSC peaks with temperature. Thus, thermal stability, decomposition behavior, composition, phase transitions, melting processes can be analyzed comprehensively and quickly using this instrument from the TGA-DSC curve. The image of the setup has been taken from the Netzsch website.

2.6 FESEM Analysis

The Field Emission Scanning Electron Microscope (FESEM) analysis was done using ZEISS Gemini SEM instrument as shown in figure 2.8. FESEM provides topographical and elemental information at very large magnifications with virtually unlimited depth of field. Compared with conventional scanning electron microscopy (SEM), FESEM produces clearer, less electrostatically distorted images with very good spatial resolution.

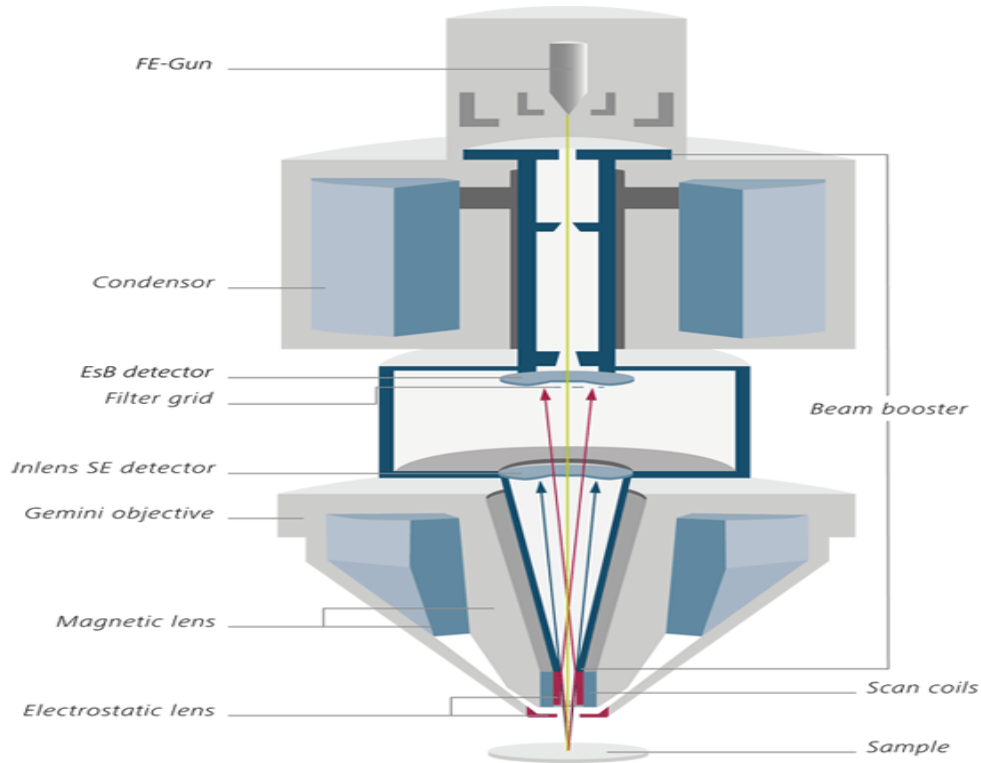


Figure 2.8: FESEM schematic diagram

Other advantages of FESEM includes the ability to examine smaller-area contamination spots at electron accelerating voltages compatible with energy dispersive spectroscopy (EDS). One can get a high-quality, low-voltage images with negligible electrical charging of samples (accelerating voltages ranging from 0.5 to 30 kilovolts) making FESESM a great tool to study the structure and composition of samples.

Principle of Operation:

A field-emission cathode in the electron gun of a scanning electron microscope provides nar-

lower probing beams at low as well as high electron energy, resulting in both improved spatial resolution and minimized sample charging and damage. In-lens field emission scanning electron microscopy (In-Lens FESEM) provides topographical information at ultra-high magnifications and images which are clearer, less electrostatically distorted than SEM, with very high spatial resolution.

Principle of Operation of EDS:

Energy dispersive spectroscopy (EDS) identifies the elemental composition of materials imaged in a scanning electron microscope for all elements with an atomic number greater than boron. As the electron beam of the SEM is scanned across the sample surface, it generates X-ray fluorescence from the atoms in its path. The energy of each X-ray photon is characteristic of the element that produced it. The EDS microanalysis system collects the X-rays, sorts and plots them by energy, and automatically identifies and labels the elements responsible for the peaks in this energy distribution.

Chapter 3

Results and discussion

3.1 Cu_2SnS_3

The sample, Cu_2SnS_3 was synthesized by sintering it at 700 °C for 12 hours and then was annealed at 680 °C for 42 hours. The structural characterization was done using powder x-ray diffraction and the scanning electron microscopy.

3.1.1 Structural characterization

Fig.3.1 shows the XRD Data of Cu_2SnS_3 which confirms the formation of the compound in a single phase of monoclinic crystal structure of space group C_1c_1 . The lattice parameter calculated was $a = 6.654 \text{ \AA}$, $b = 11.507 \text{ \AA}$, $c = 6.643 \text{ \AA}$ and the angle $\beta = 109.5^\circ$. The volume of the unit cell was found out to be 479.493 \AA^3 . To see the stability of the sample at high temperatures, the high temperature XRD was done till 650 °C as shown in the figure 3.2 (a). The result showed no change in the structure of the sample till 650 °C but only the expansion in the lattice leading to the shift of the peaks towards lower angle with increasing temperature. Figure 3.2 (b) shows the peak (hkl) at $2\theta=28.5^\circ$ showing the leftward shift of the peaks.

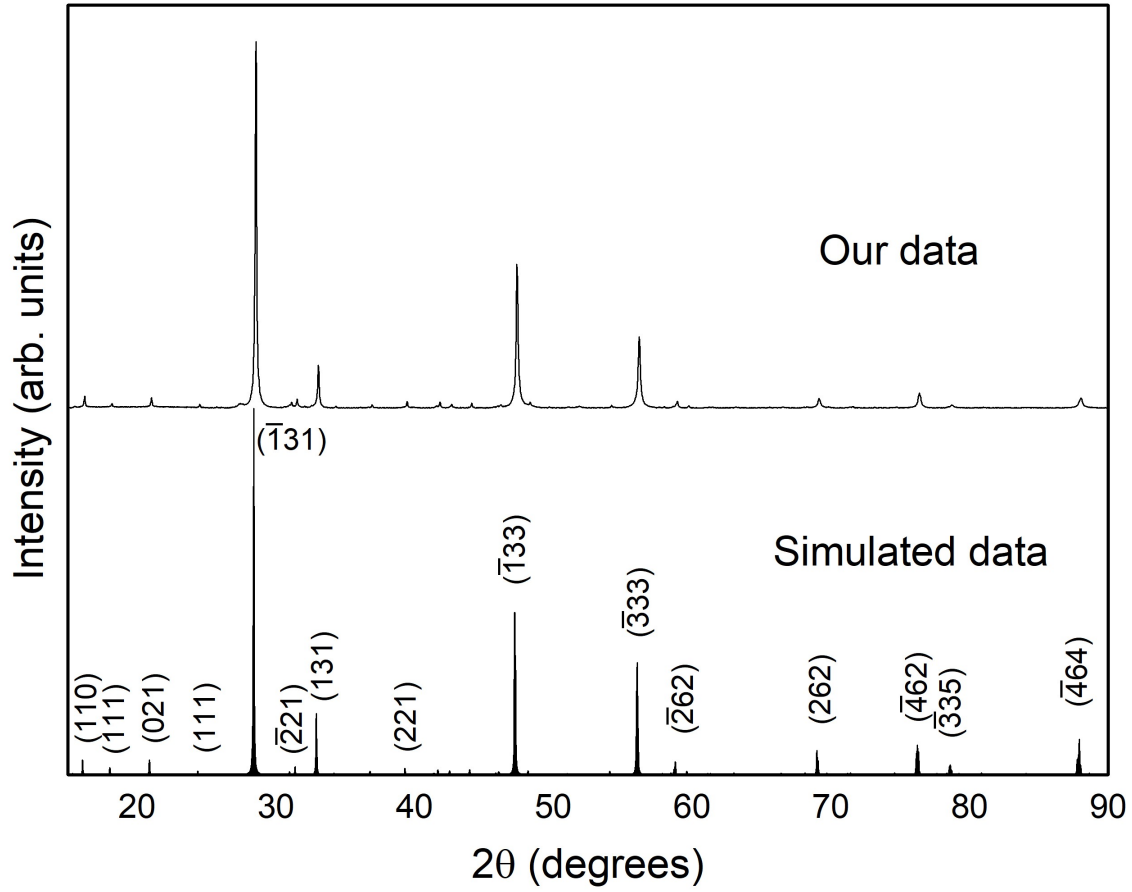
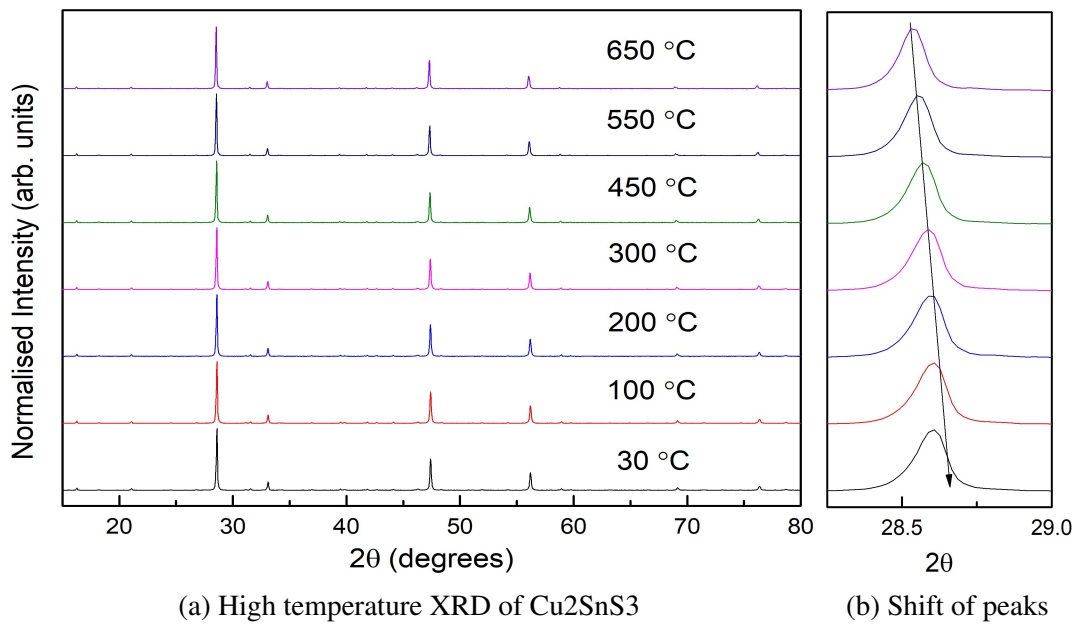


Figure 3.1: XRD of Cu_2SnS_3



(a) High temperature XRD of Cu_2SnS_3

(b) Shift of peaks

Figure 3.2: HTXRD of Cu_2SnS_3

The lattice parameters, a, b, c and the volume of the cell was calculated to see their behavior with the increase in temperature. It is shown in the figure 3.3. The "a" and "b" parameter of the lattice has an abnormal behavior at 200 °C, where "a" parameter suddenly decreases and "b" parameter suddenly increases. The "c" parameter however shows continuous increase and hence, an overall linear increase can be seen in the volume of the unit cell of the lattice. The linear increase of the unit cell volume with temperature shows that the lattice expands as one goes on increasing the temperature.

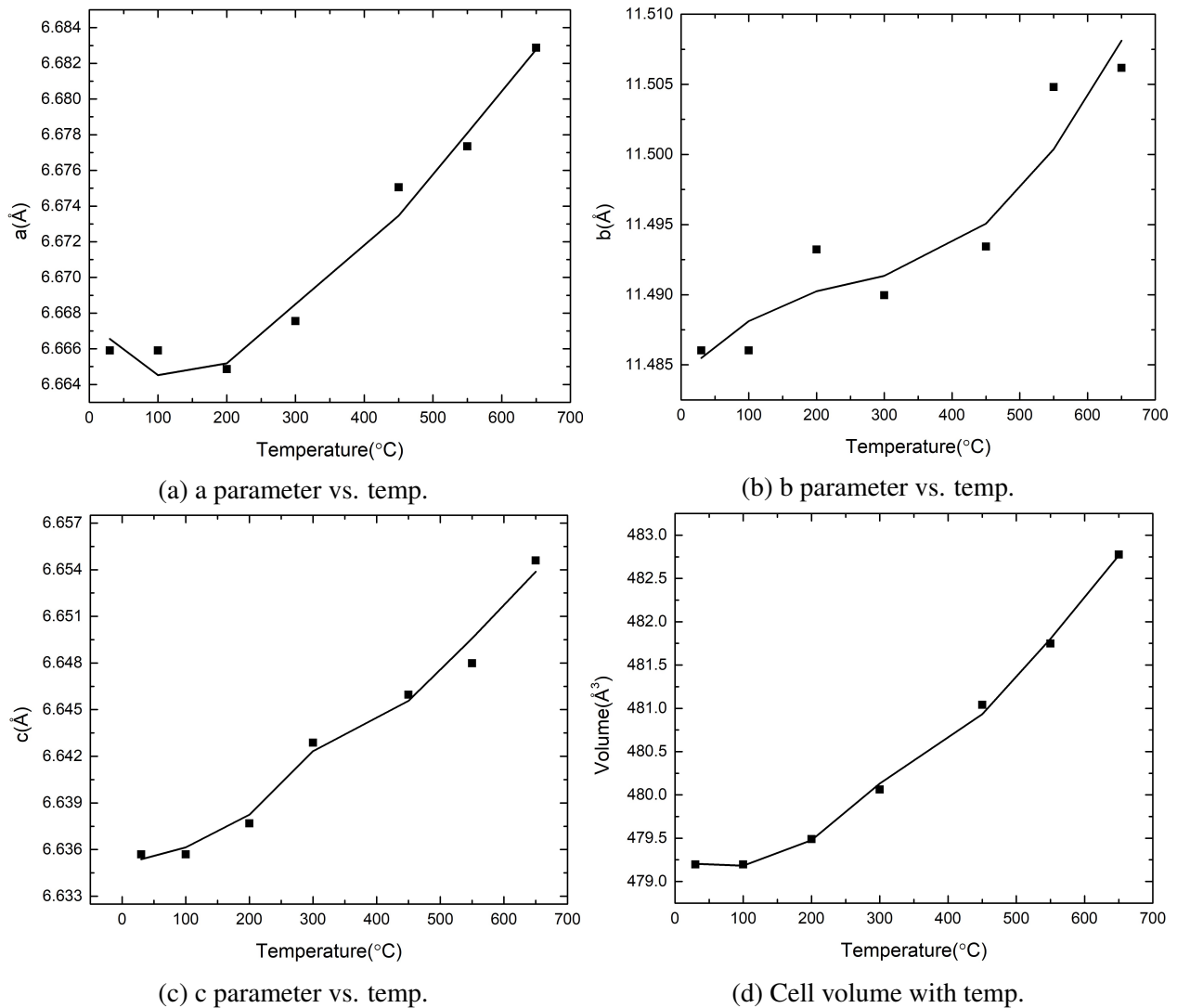


Figure 3.3: Lattice parameters comparison with temperature

3.1.2 TGA DSC measurement

The TGA-DSC was also done, till 800 °C to confirm the stability at high temperatures. The graph in the figure 3.4 (a) shows that the sample loses more than 10% of the mass and the majority of the mass loss happens after 700 °C. Since, sulfur is very volatile, the mass loss is attributed to the loss of sulfur only. The sulfur in Cu_2SnS_3 comprises of 28% of the total mass. Hence, a loss of 10% is a huge loss and with respect to sulfur, more than 35% of all the sulfur present is lost. This changes the sample completely and hence is clearly visible as a peak showing freezing in the DSC curve in figure 3.4 (b) at temperature around 500 °C while cooling the sample. The sample melted and then got solidified on to the crucible which was removed by cleaning the crucible in aqua regia. The measurements were done in Argon atmosphere as Purge gas with gas flow of 20 mL/min and the nitrogen gas as the protective gas for balance with a flow rate of 20 mL/min.

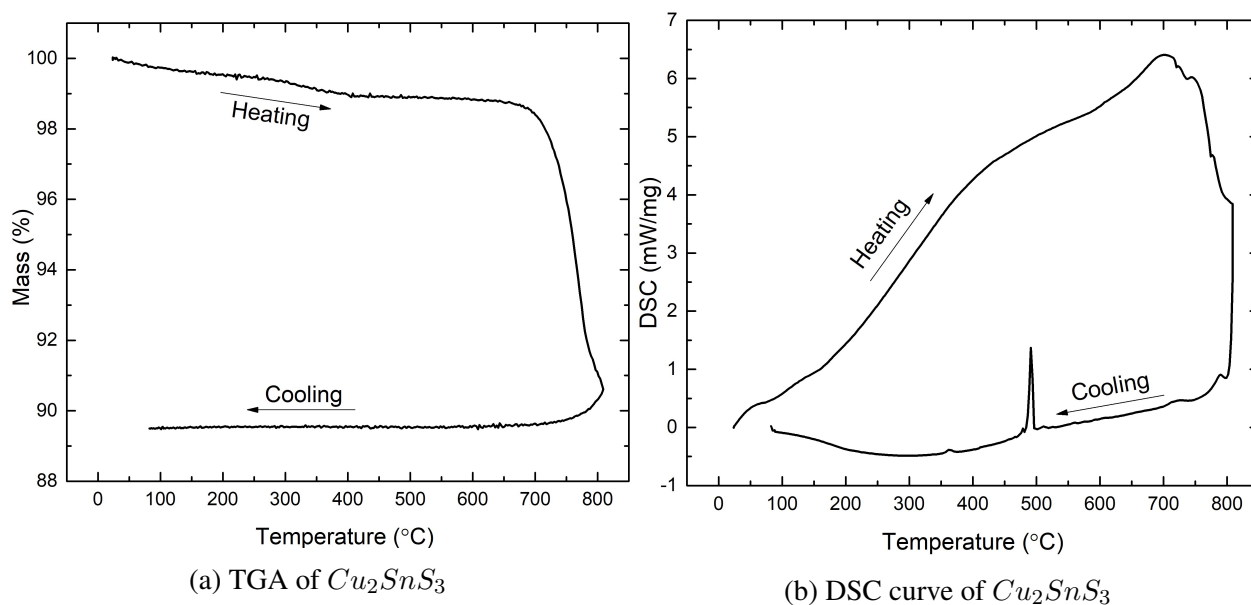


Figure 3.4: TGA-DSC of Cu_2SnS_3

3.1.3 FESEM analysis

The FESEM was done on a flat polished piece of the sample to know the morphology and the composition of the sample. The FESEM image in figure 3.5 (left) shows the small pores indicating

the sample being less dense. On further zooming into the sample we could see that the particles fused together as if they have melted while annealing it as shown in figure 3.5 (right). The EDS analysis was done on several points and then averaged to give the composition as $Cu_{1.89}Sn_{1.01}S_{3.09}$. This is in good agreement with the expected stoichiometry considering the error we get in the EDS analysis.

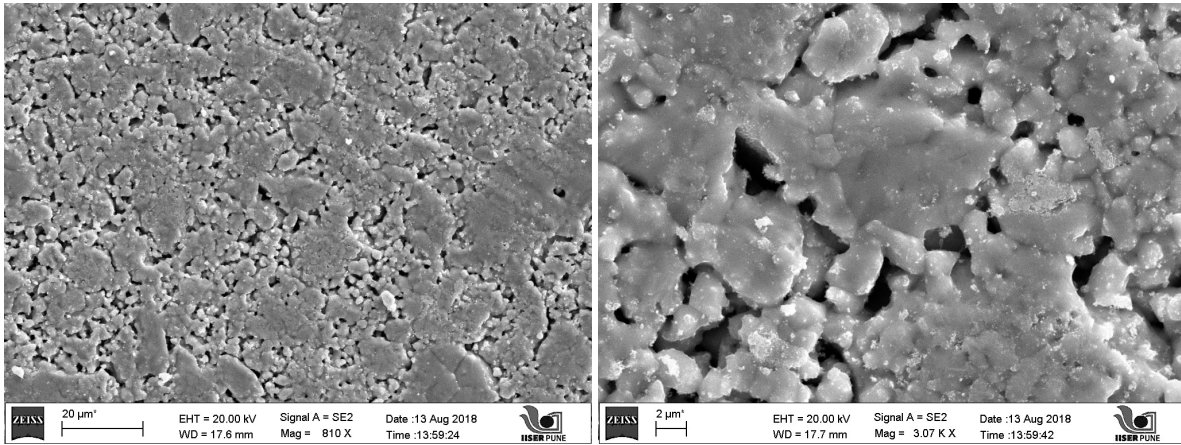


Figure 3.5: FESEM images of Cu_2SnS_3

3.1.4 LFA and LSR measurement

The LFA measurement was done on an 8mm pellet of thickness 0.65 mm. The density of the sample when compared to the theoretical density of 4.71 g/cm^3 is 81% while the density of the reported sample was 97% from the paper, "Cobalt doping in Cu_2SnS_3 " by Zhao et. al. [10]. Since, the value of thermal conductivity depends on the density of the sample, the lower value of density for our sample leads to a decrease in the value of thermal conductivity than the reported sample. From figure 3.6, the thermal conductivity of the sample decreases with temperature and at room temperature the maximum thermal conductivity of 2 W/m/K is achieved for our sample of Cu_2SnS_3 . Then, the value of κ goes to a value, as low as 0.6 W/m/K at 450 °C.

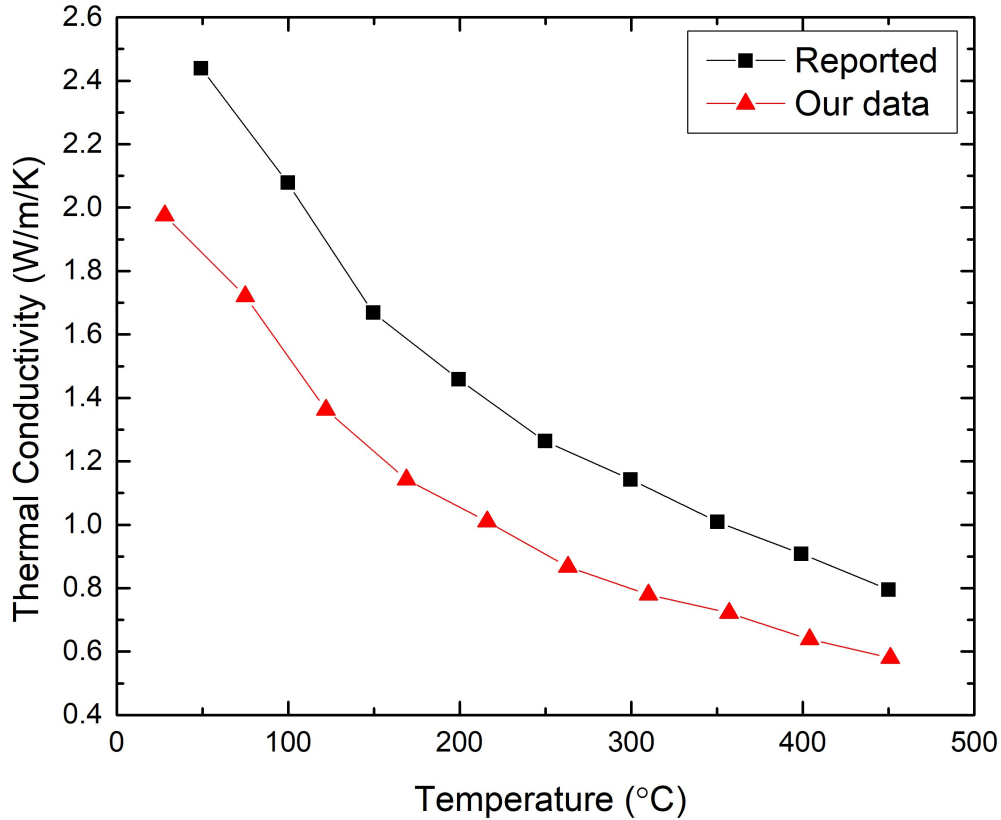


Figure 3.6: Thermal Conductivity vs. Temperature of Cu_2SnS_3

After this, the LSR measurement was done on a 7mm long sample till 450 °C. Although LFA data matched with the reported data, the LSR data i.e. the electrical conductivity and the seebeck coefficient data was not matching as shown in the figure 3.7 (a) and (b) for 1st pellet. Hence, the measurement was repeated on a different pellet of the same batch labelled as "2nd pellet" in the graph. The data of the 2nd pellet matched well with the 1st pellet but again not with the reported data. The reported data has a maximum Seebeck value of 420 $\mu V/K$ value at 300 °C while our sample has shown a maximum Seebeck value of more than 700 $\mu V/K$ at 350 °C. The electrical conductivity as well doesn't match and is less than the reported value. For the reported sample, the maximum electrical conductivity value is close to 7 S/cm while it is 3.25 S/cm for our sample at 150 °C. The electrical conductivity of our sample becomes close to zero after 400 °C.

The overall power factor showed a similar trend with a maximum of 0.55 $\mu W/cm/K^2$ at 250 °C for our sample while the reported data showed a maximum power factor of more than 0.75 $\mu W/cm/K^2$ at 150 °C as shown in figure 3.7 (c).

The maximum ZT obtained for our sample is close to 0.035 at 300 °C and is almost same compared to the reported sample's data. The overall figure of merit, ZT of the sample showed similar value till 300 °C and after this temperature, the value of ZT for our sample goes down sharply as shown in the figure 3.7 (d).

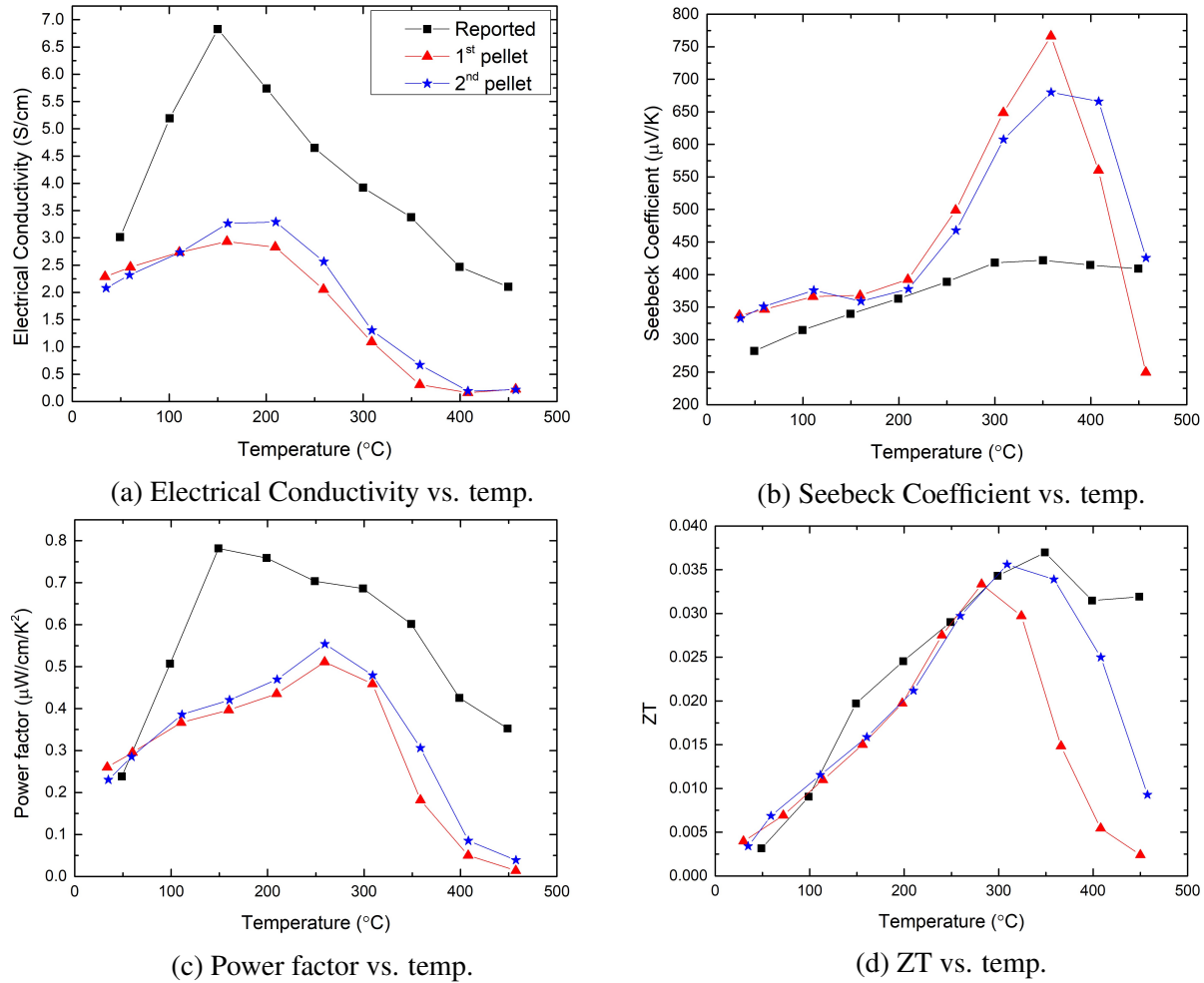


Figure 3.7: LSR measurement comparison with reported value

3.2 $CuCo_2S_4$

After this, another sample studied was from the spinel family, AB_2X_4 , with A=Cu, B=Co and X=S i.e. $CuCo_2S_4$, a thiospinel. Later on, the off-stoichiometric samples were studied by

creating anti-site disorder in the sample. First of all we tried it by synthesizing $Cu_{0.9}Co_{2.1}S_4$ and $Cu_{1.1}Co_{1.9}S_4$. But, we could not get rid of the extra CoS_2 phases in the $Cu_{1.1}Co_{1.9}S_4$ sample while $Cu_{0.9}Co_{2.1}S_4$ formed easily after second sintering. The structural and thermoelectric properties of all such off-stoichiometric samples are studied in this section starting from $CuCo_2S_4$ to Co_3S_4 . The thermoelectric measurements of some of the end members of this series could not be done due to instrument breakdown.

3.2.1 Structural characterization

The XRD data of $CuCo_2S_4$ is shown in figure 3.8. The comparison of our sample's xrd data with the simulated data confirms the single phase of $CuCo_2S_4$.

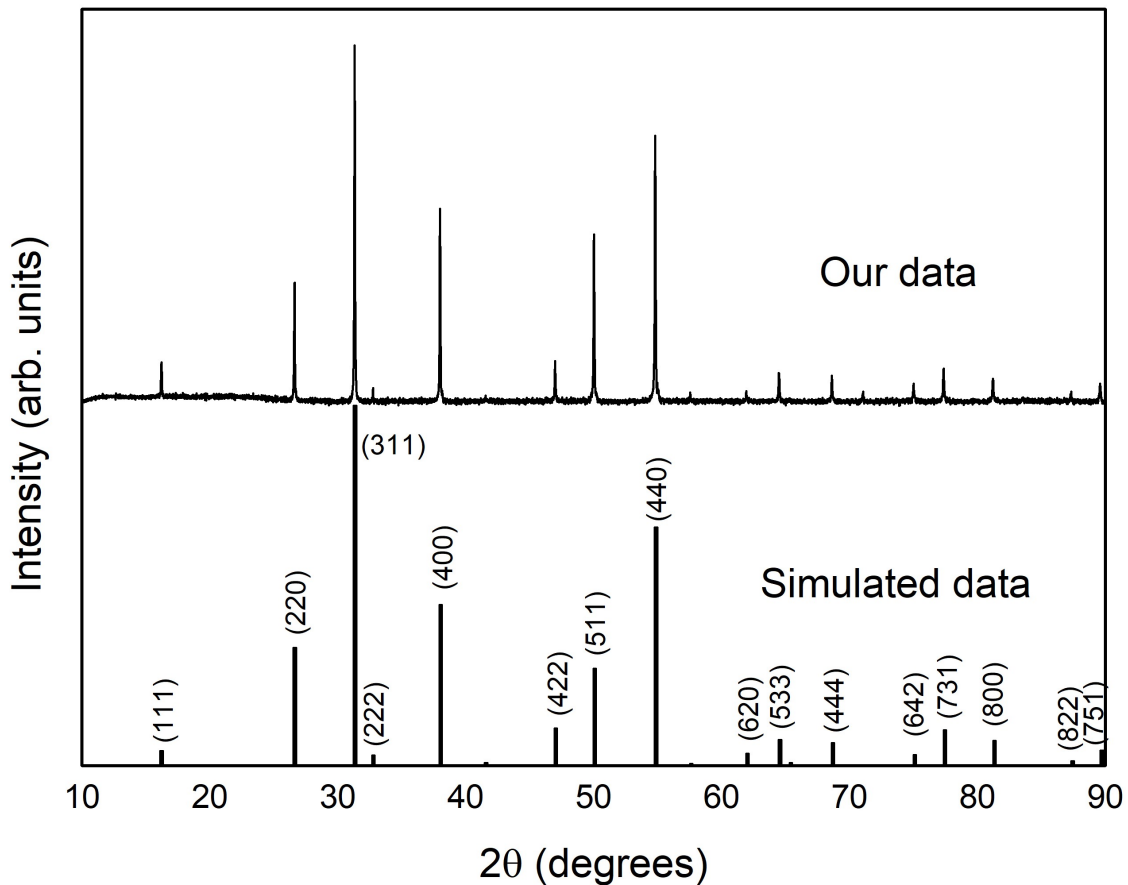


Figure 3.8: XRD plot of $CuCo_2S_4$

Later on, other off-stoichiometric samples were synthesized by replacing Co in place of Cu in

$CuCo_2S_4$. The XRD data of all such samples are shown in figure 3.9 (a). In figure 3.9 (b), the rightward shifts in the peak at 2θ around 31° shows a normal behavior of lattice contraction upon replacing a smaller atom of cobalt (atomic radius=125 pm) in place of copper (atomic radius=128 pm). The lattice parameter were calculated by the unit cell software by taking the positions of several xrd peaks. The lattice parameter shown in the figure 3.10 confirms the linear decrease in the value as one replaces a bigger atom, copper with a smaller one of that of cobalt. The calculated value of lattice parameter of $CuCo_2S_4$ was 9.47 Å and 9.401 Å for Co_3S_4 and matches well with the reported value of 9.478 Å for $CuCo_2S_4$ and 9.406 Å for Co_3S_4 .

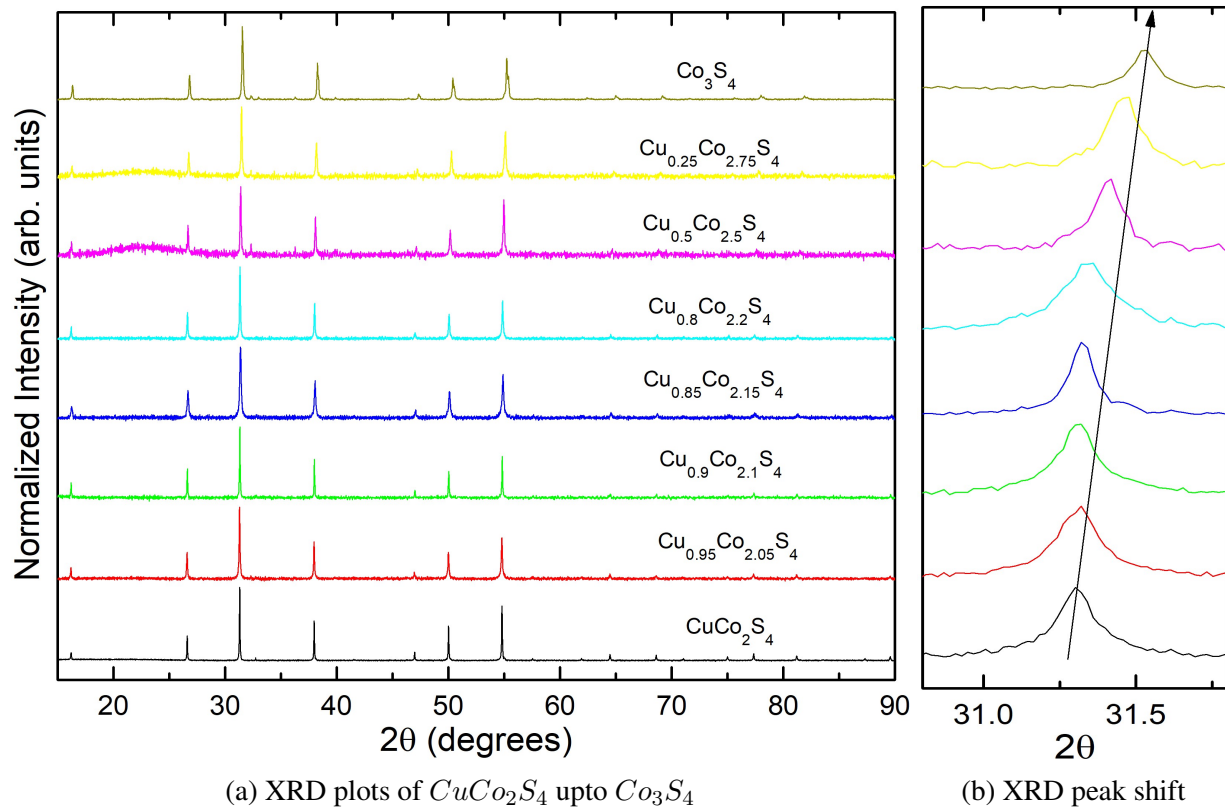


Figure 3.9: XRD of $CuCo_2S_4$ to Co_3S_4 along with the off-stoichiometric samples.

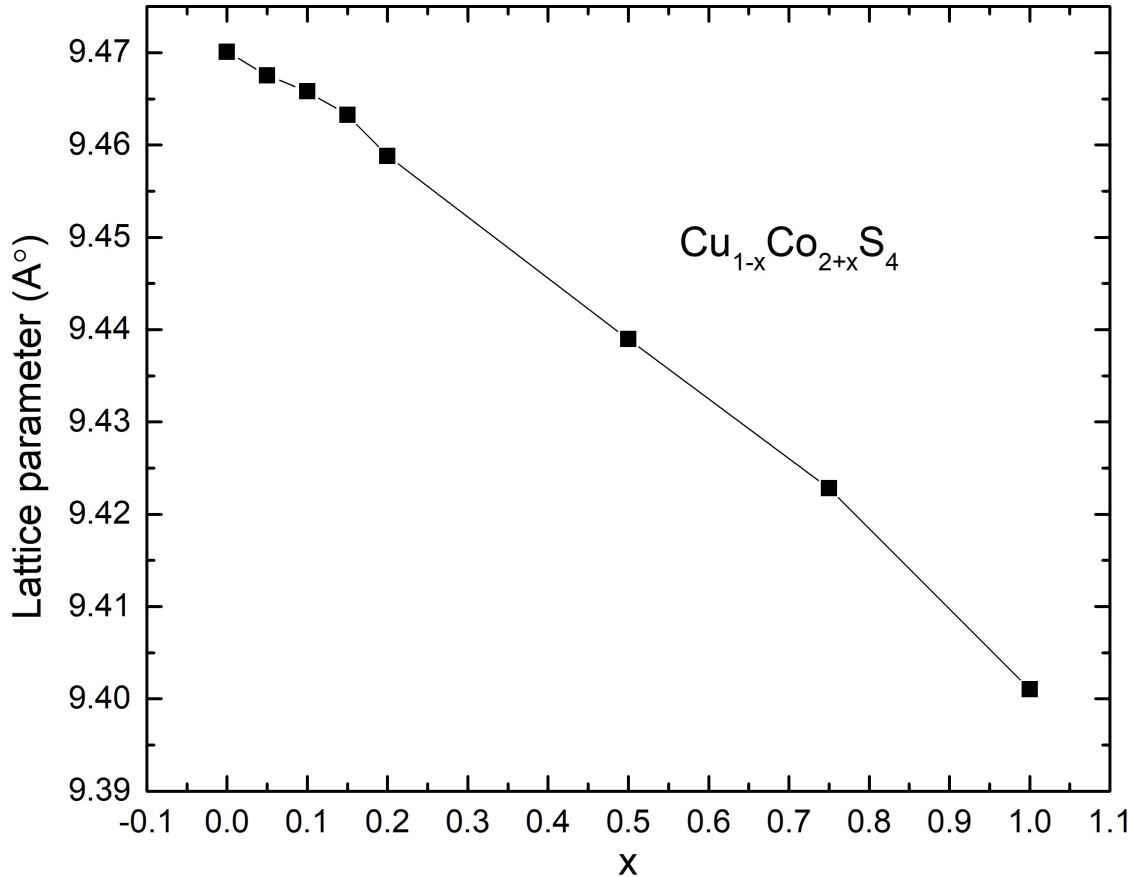


Figure 3.10: lattice parameter variation with addition of Cobalt

3.2.2 TGA-DSC measurement

Before proceeding for the thermoelectric measurements, we did the TGA-DSC on the $CuCo_2S_4$ sample to ensure that the maximum measurement temperature doesn't involve a huge mass loss or any other major changes in the sample. The measurement was done till 700 °C under Argon flow as purge gas of 60mL/min and nitrogen flow as protective gas of 40 mL/min. The data in figure 3.11 shows a mass loss of around 7% and most of the mass loss was seen after 500 °C. The mass loss is due to sulfur loss at higher temperatures. Thus it was decided to synthesize another sample of $CuCo_2S_4$ and the off-stoichiometric samples at 500 °C only to avoid loss of sulfur at higher temperatures. The DSC data does not show any sharp peak and thus no signs of melting or decomposition was observed. Hence, the thermoelectric measurements were done till 450 °C since till there, just 1% mass loss is observed.

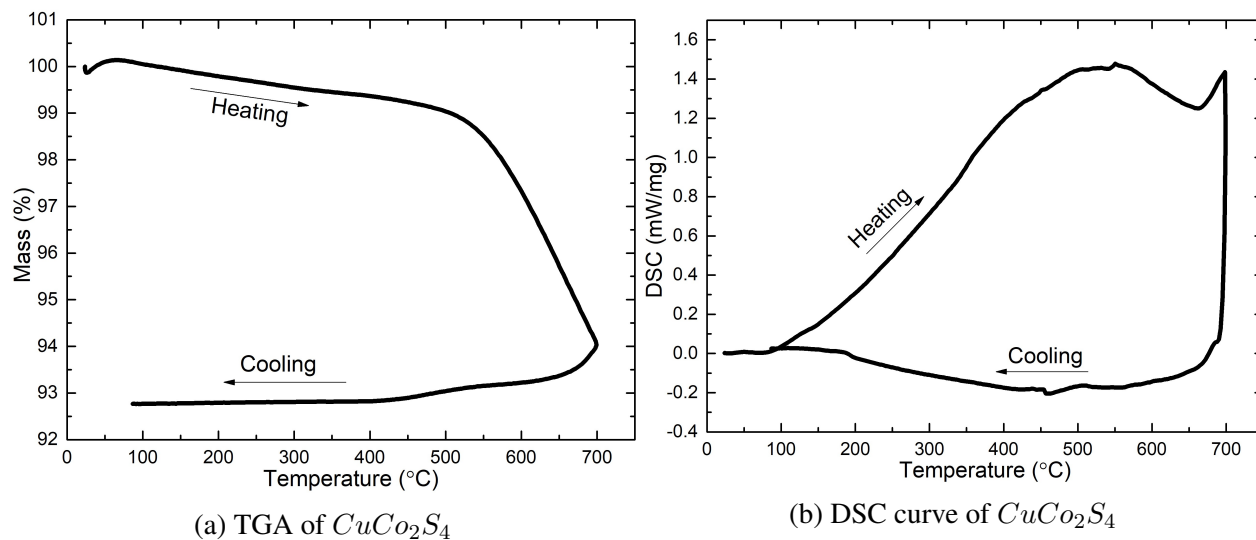


Figure 3.11: TGA-DSC data of $CuCo_2S_4$

3.2.3 FESEM Analysis

The FESEM images of all the synthesized samples from $CuCo_2S_4$ to Co_3S_4 was done to see the density of the sample, the morphology and the grain size as well. The images are shown in the figures 3.12-3.14.

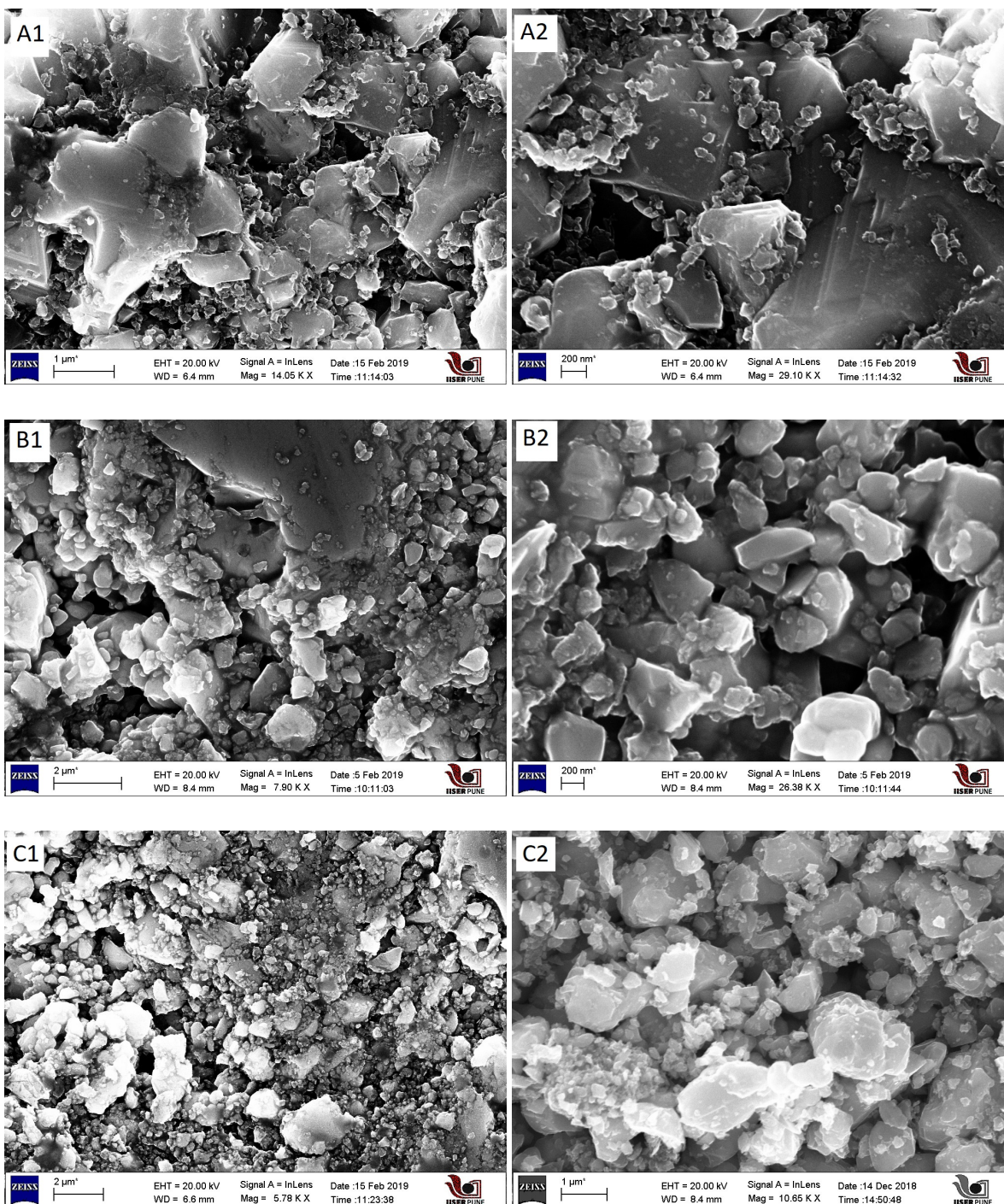


Figure 3.12: The figures A-C represents the FESEM images of the samples: A1, A2: $CuCo_2S_4$, B1, B2: $Cu_{0.95}Co_{2.05}S_4$, C1, C2: $Cu_{0.9}Co_{2.1}S_4$,

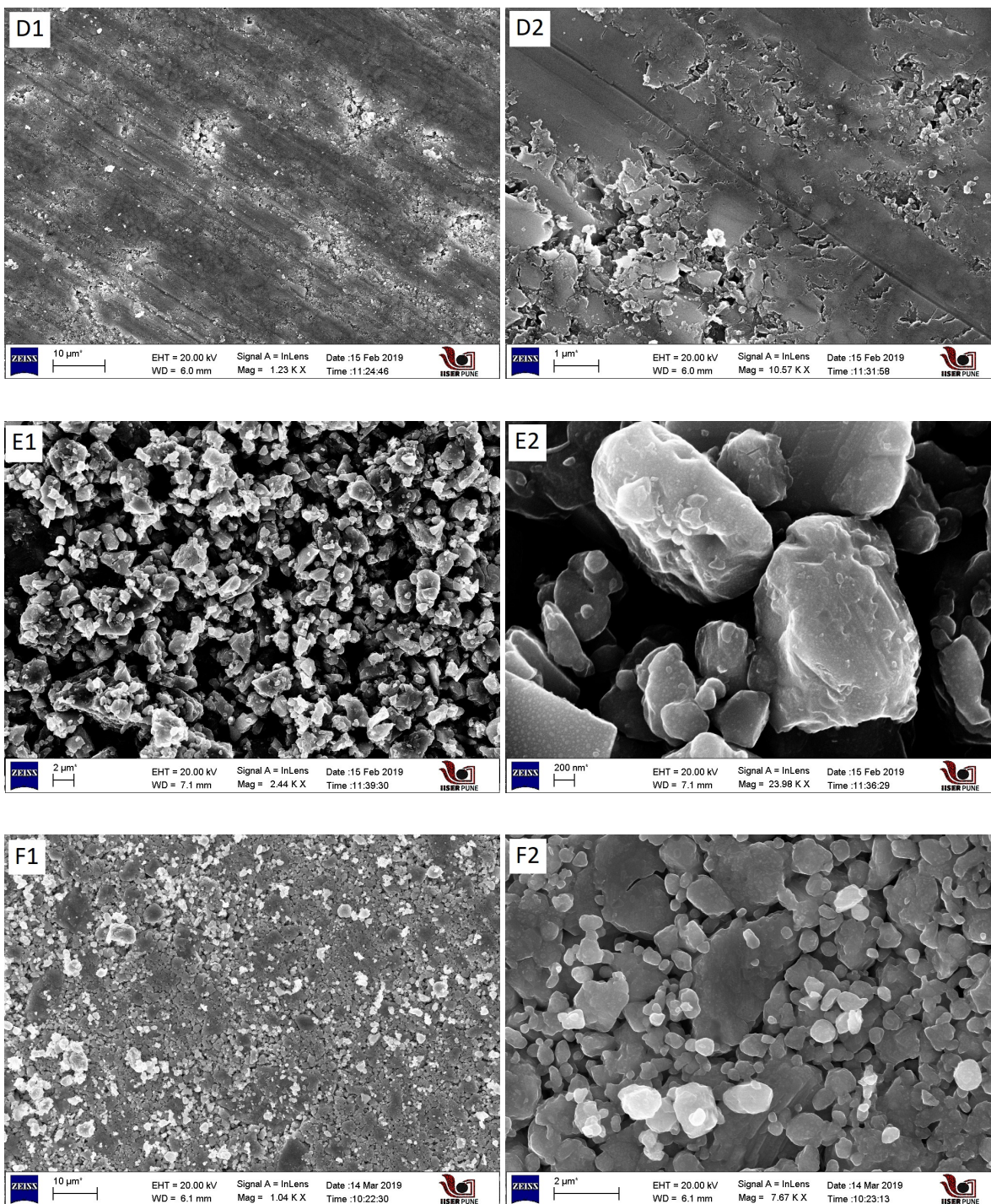


Figure 3.13: The figures D-F represents the FESEM images of the samples: D1, D2: $Cu_{0.85}Co_{2.15}S_4$, E1, E2: $Cu_{0.8}Co_{2.2}S_4$, F1,F2: $Cu_{0.5}Co_{2.5}S_4$

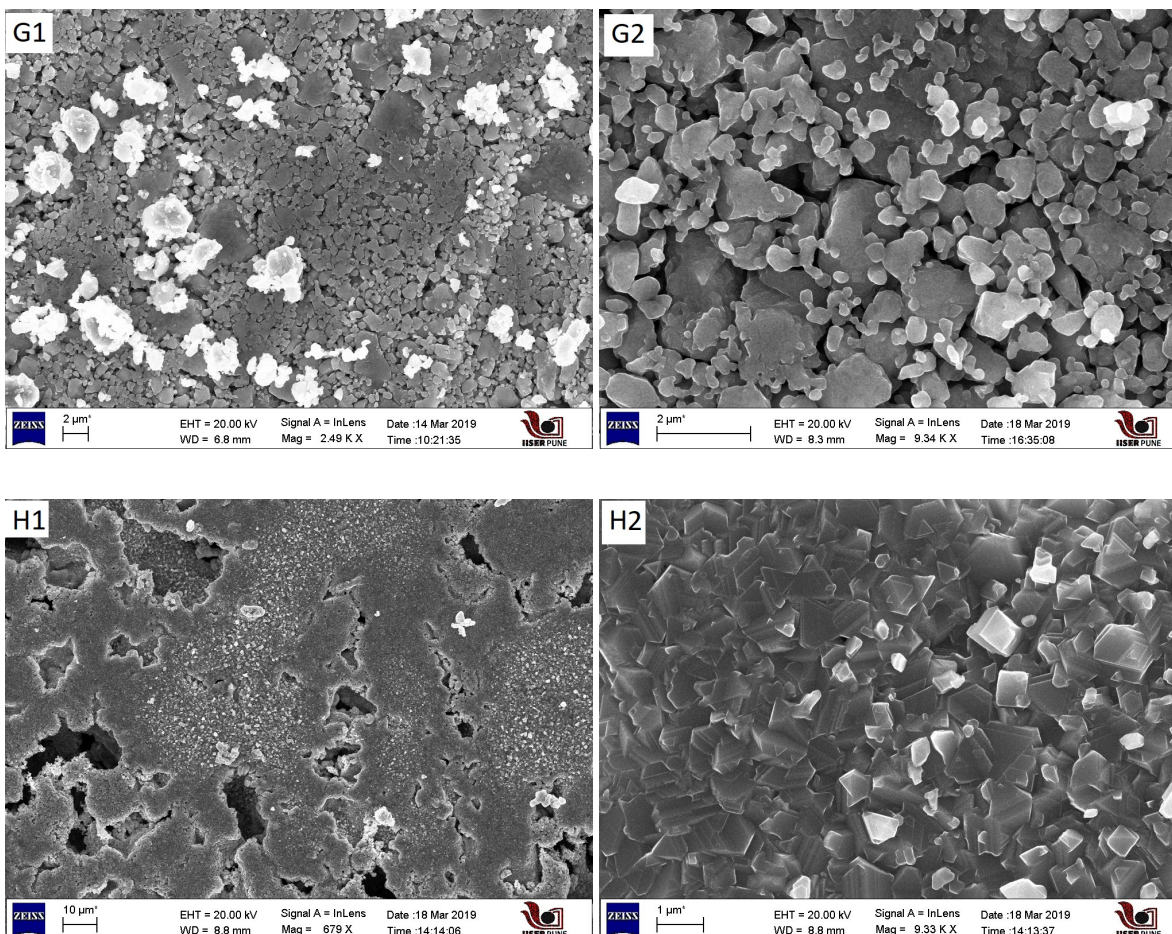


Figure 3.14: The figures G-H represents the FESEM images of the samples: G1, G2: $Cu_{0.25}Co_{2.75}S_4$, H1, H2: Co_3S_4

The presence of pores in the samples shows that the sample synthesized were less dense. The images show the variation in the grain size of the samples from few μm to few hundreds of nm. One can also see the layered structure in the $CuCo_2S_4$ sample in A1 and A2 image of figure 3.12. Also, the Co_3S_4 particles looked quite different and lots of layered structure are clearly visible in H2 image of figure 3.14.

The Energy Dispersive X-Ray Spectroscopy (EDS) data was recorded to find out the stoichiometry of the samples synthesized and also to detect if there are any impurity phase present. The EDS data was taken over various different area on the sample and then averaged to find the stoichiometry of the sample. This gives the atomic percentage of the elements present over that area based

on the energy and the intensity of the characteristic x-ray received from that area or a point. The averaged data over more than 10-18 such area for all the samples is shown in figure 3.15. Taking the error due to EDS into consideration, the sample can be considered to have formed in desired stoichiometry.

Sample	No. of points	Cu:Co (Expected)	Cu:Co (Observed)
CuCo_2S_4	15	1:2	[1]:[2±0.1]
$\text{Cu}_{0.95}\text{Co}_{2.05}\text{S}_4$	12	1:2.2	[1]:[2.1±0.1]
$\text{Cu}_{0.9}\text{Co}_{2.1}\text{S}_4$	18	1:2.3	[1]:[2.3 ± 0.1]
$\text{Cu}_{0.85}\text{Co}_{2.15}\text{S}_4$	11	1:2.5	[1]:[2.5]
$\text{Cu}_{0.8}\text{Co}_{2.2}\text{S}_4$	13	1:2.7	[1]:[2.8 ± 0.1]
$\text{Cu}_{0.5}\text{Co}_{2.5}\text{S}_4$	10	1:5	[1]:[5.2 ± 0.1]
$\text{Cu}_{0.25}\text{Co}_{2.75}\text{S}_4$	13	1:11	[1]:[11.4 ± 0.2]

Figure 3.15: EDS Analysis of compounds

3.2.4 LFA and LSR measurement

The LFA measurements were done in vacuum on 6mm or 8mm pellets with density as mentioned in the figure 3.17. From the figure 3.16, we can see that the thermal conductivity of the samples remain almost constant throughout the temperature range upto 450 °C. For $\text{Cu}_{0.8}\text{Co}_{2.2}\text{S}_4$, the thermal conductivity is 0.75 W/m/K at room temperature and the values increases as one increases Cu content and goes towards the CuCo_2S_4 sample. But the sample $\text{Cu}_{0.9}\text{Co}_{2.1}\text{S}_4$ doesn't fall into this trend and achieves a high thermal conductivity of around 3W/m/K. Since, thermal conductivity is dependent on the density of the sample, figure 3.17 shows the densities of the samples. One can see that the densities for all the samples are nearly the same. The density of the off stoichiometric samples (in %) is with respect to the pristine sample, CuCo_2S_4 .

The thermal conductivity data showed a hysteresis and the heating and cooling data were not overlapping after the 1st run. There was a significant mass loss in the sample after the first run is done on the sample. So, the measurement was repeated on each of the samples and the heating data of second run has been taken. The mass loss is attributed to the sulfur loss at higher temperatures.

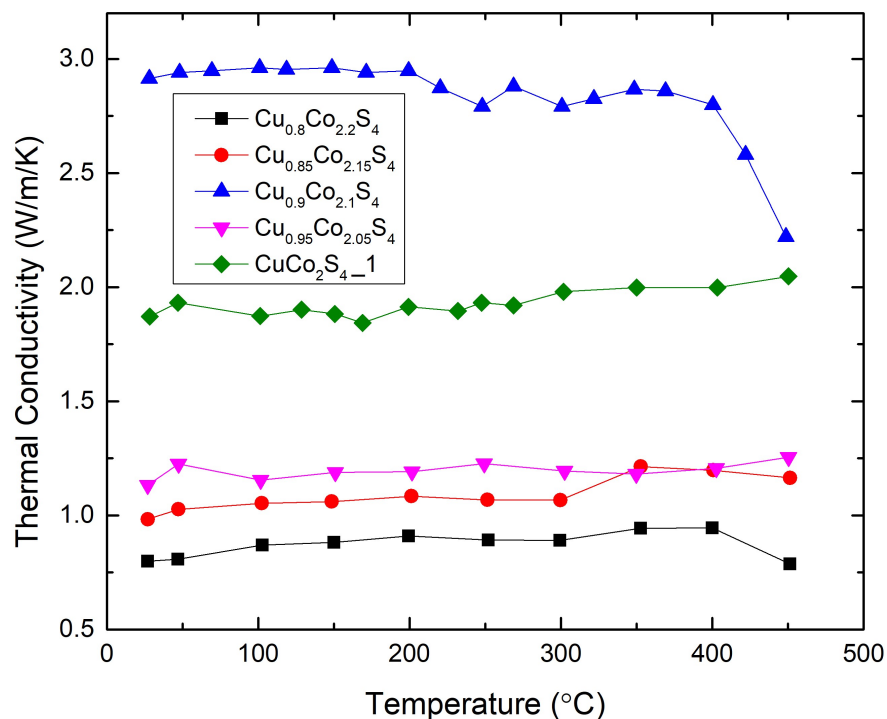


Figure 3.16: Thermal Conductivity data of CuCo_2S_4 and the off-stoichiometric samples

and plotted as shown in the figure 3.18. The XRD was done on the samples after the LFA measurement and it didn't show any phase change of the samples. So, although there is a significant loss of the sulfur from the sample, it is not abruptly changing the phase of the sample.

Density (g/cm ³):	
$\text{Cu}_{0.8}\text{Co}_{2.2}\text{S}_4$	=3.04 =63%
$\text{Cu}_{0.85}\text{Co}_{2.15}\text{S}_4$	=3.37 =70%
$\text{Cu}_{0.9}\text{Co}_{2.1}\text{S}_4$	=3.61 =75%
$\text{Cu}_{0.95}\text{Co}_{2.05}\text{S}_4$	=3.67 =76%
CuCo_2S_4	=3.29 =68%

Figure 3.17: Density of samples for LFA

Such a significant mass loss is not seen in the LSR measurements. The only difference between the LFA and LSR measurement is the atmosphere in which the measurement is done. While LFA was done in vacuum, LSR measurements were done in Helium atmosphere. At higher temperature, it would be easier for sulfur to escape in vacuum than when it is surrounded by helium gas.

The LSR measurements were reproducible in the heating and cooling run and hence was averaged

From the LSR measurements, one can see that the electrical conductivity of the sample decreases with temperature, showing a metal like behavior. The high values of electrical conductivity (800 S/cm-2300 S/cm) would favor the increase in ZT. Here also, the $\text{Cu}_{0.9}\text{Co}_{2.1}\text{S}_4$ sample doesn't follow the trend and has the highest electrical conductivity (2300 S/cm at RT) among all the samples.

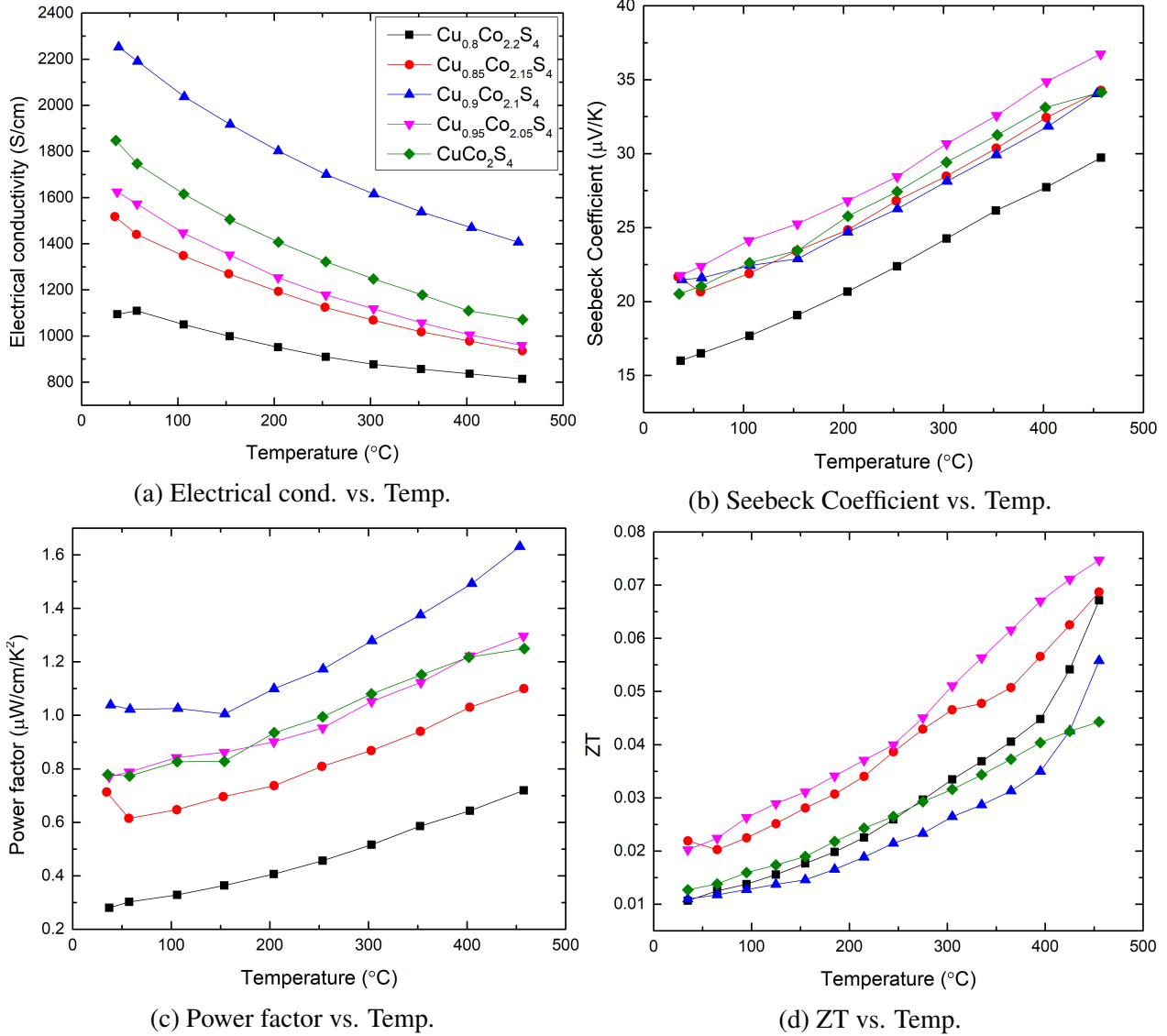


Figure 3.18: LSR measurements for $CuCo_2S_4$ and the off-stoichiometric samples

But the Seebeck coefficient remains almost the same for the different samples. The Seebeck coefficient for these samples are not very high and it ranges from around $20 \mu V/K$ at room temperature to $35 \mu V/K$ at $450^{\circ}C$. Among all of the samples, $Cu_{0.8}Co_{2.2}S_4$ sample has the lowest value for the Seebeck Coefficient and it ranges from $15 \mu V/K$ to $30 \mu V/K$ at $450^{\circ}C$. The power factor for the samples shows the same trend as for the electrical conductivity as shown in figure 3.18(c). The Power factor of the pristine sample, $CuCo_2S_4$ ranges from $0.8 \mu W/cm/K^2$ at room temperature to more than $1.2 \mu W/cm/K^2$. The power factor is the maximum for the $Cu_{0.9}Co_{2.1}S_4$ sample, which

increases from $1 \mu\text{W}/\text{cm}/\text{K}^2$ at room temperature to $1.7 \mu\text{W}/\text{cm}/\text{K}^2$ at 450°C .

The figure of merit, ZT for the sample was in the range from 0.01 to 0.075. ZT for CuCo_2S_4 increased from 0.01 to .045 at 450°C . The maximum ZT of 0.075 was obtained for $\text{Cu}_{0.95}\text{Co}_{2.05}\text{S}_4$ sample at 450°C as shown in figure 3.18 (d).

3.3 CuZr_2S_4

The samples, CuZr_2S_4 and CuCoZrS_4 were synthesized by heating the precursors slowly @ $30^\circ\text{C}/\text{hr}$. to 350°C and then to 750°C @ $4^\circ\text{C}/\text{hr}$. It was kept at 750°C for a week and then cooled slowly @ 30°C to room temperature. The sample obtained was very fine and dark black powder and a small ingot.

3.3.1 XRD characterization

The CuZr_2S_4 sample got synthesized and the XRD data shown in the figure 3.19 confirms its single phase and the lattice parameter calculated was 10.371 \AA . The other sample, CuCoZrS_4 could not be synthesized and the xrd peaks consists of phases of CuZr_2S_4 , CuCo_2S_4 and CoS_2 as shown in the figure 3.20.

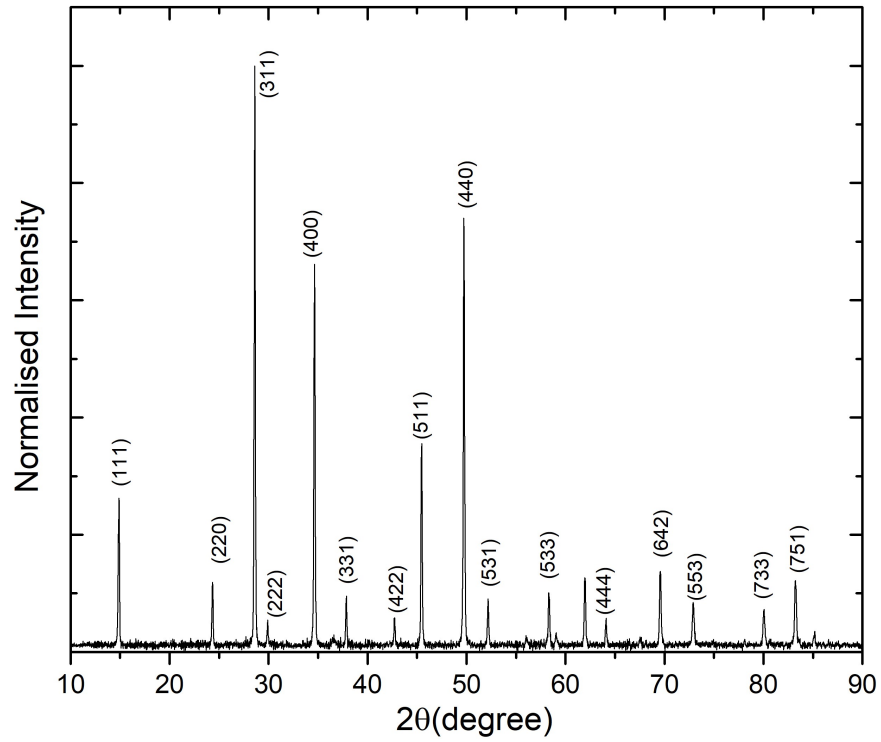


Figure 3.19: XRD of $CuZr_2S_4$

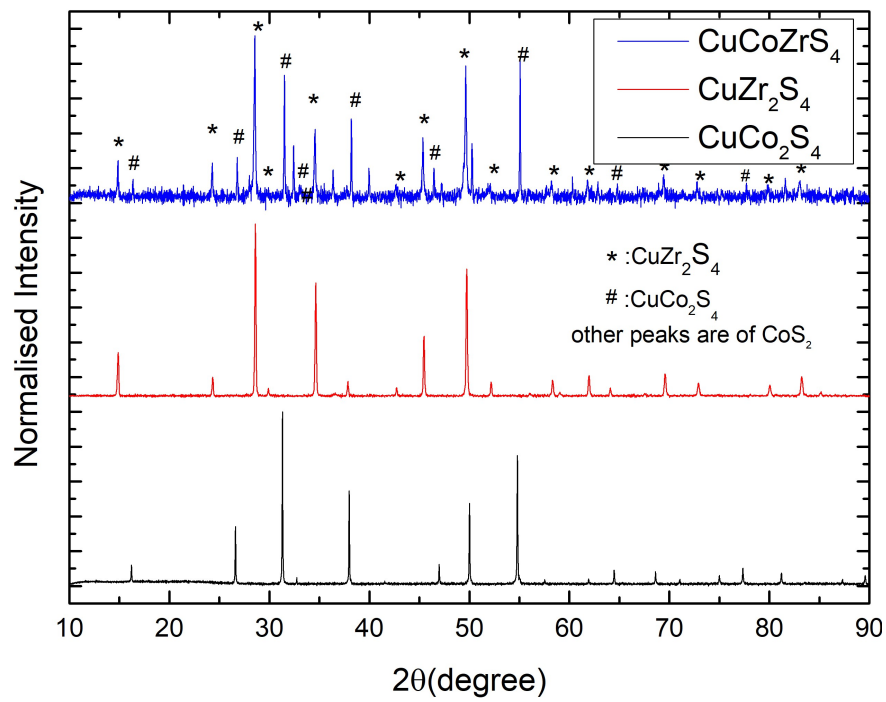


Figure 3.20: XRD of $CuCoZrS_4$

3.3.2 FESEM Analysis

A small piece of the ingot from $CuZr_2S_4$ was taken out for the FESEM images of the samples as shown in the figure 3.21. The first image shows some flower like structures all across the sample. On further zooming into one of those structures, we could see the layering in the sample stacked one above the other. since, this piece was taken out from as grown crystal, the surface was not flat and hence, the EDS analysis was not done. The sample is to be pelletized for annealing for further FESEM analysis and the thermoelectric measurements.

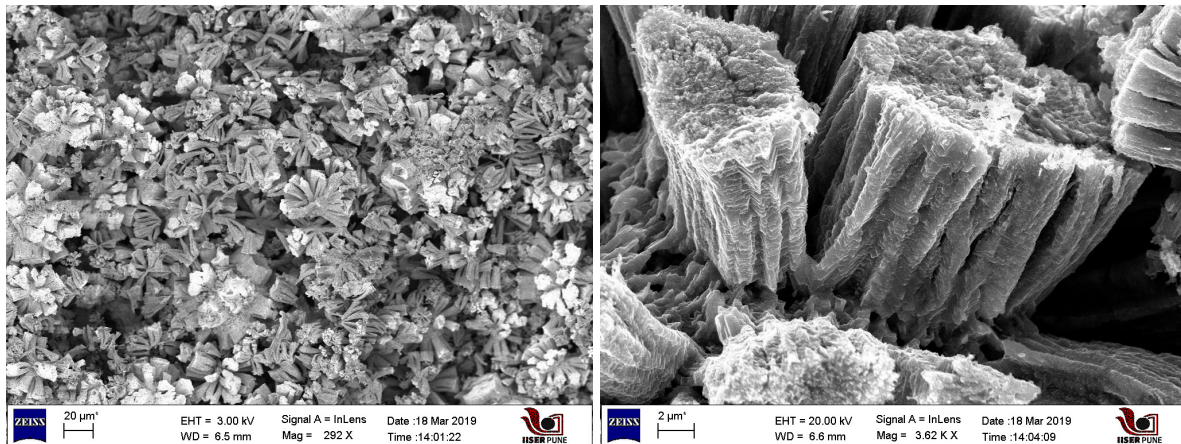


Figure 3.21: FESEM images, $CuZr_2S_4$

Chapter 4

Conclusion

The sample Cu_2SnS_3 was synthesized and the thermal conductivity measurements matched well with the reported data. But the electrical conductivity and the Seebeck Coefficient data did not match well with the reported data. The high temperature x-ray diffraction of the sample showed a linear expansion of the volume of the lattice. The other sample, $CuCo_2S_4$ all the way upto Co_3S_4 was synthesized and along with it, the off-stoichiometric samples were also synthesized by replacing Co in place of Cu. Replacing Cu at the Co site in synthesizing $Cu_{1.1}Co_{1.9}S_4$ did not work as there were prominent extra phases of CoS_2 present. The $CuCo_2S_4$ sample worked out to be highly conductive sample with conductivity close to 1900 S/cm at room temperature. The Seebeck coefficient of the samples remained almost the same throughout in the range of 20-35 $\mu V/K$ for the temperature range of 30 °C to 450 °C. The sample $Cu_{0.9}Co_{2.1}S_4$ showed an unusual trend from all and has shown the highest value of power factor as well of 1-1.7 $\mu W/cm/K^2$ in the measured temperature range . The ZT obtained was in the range of 0.04 at 30 °C to 0.075 at 450 °C and the highest value of 0.075 was obtained for the $Cu_{0.95}Co_{2.05}S_4$ sample. The other samples, $Cu_{0.5}Co_{2.5}S_4$, $Cu_{0.25}Co_{2.75}S_4$, Co_3S_4 and $CuZr_2S_4$ could not be measured due to instrument breakdown. Thus, though the ZT is not very high for the $CuCo_2S_4$ and off-stoichiometric samples, doping with Sn, Sb at Co site can help in improving its thermoelectric properties. Other sample like $CuZr_2S_4$ is also expected to have higher Seebeck coefficient.

Bibliography

- [1] Zhen-Hua Ge, Peng Qin, DongSheng He, Xiaoyu Chong, Dan Feng, Yi-Hong Ji, Jing Feng, and Jiaqing He. Highly enhanced thermoelectric properties of bi/bi₂s₃ nanocomposites. *ACS applied materials & interfaces*, 9(5):4828–4834, 2017.
- [2] Zhen-Hua Ge, Li-Dong Zhao, Di Wu, Xiaoye Liu, Bo-Ping Zhang, Jing-Feng Li, and Jiaqing He. Low-cost, abundant binary sulfides as promising thermoelectric materials. *Materials Today*, 19(4):227–239, 2016.
- [3] T Oda, M Shirai, N Suzuki, and K Motizuki. Electronic band structure of sulphide spinels CuM_2S_4 (m= co, rh, ir). *Journal of Physics: Condensed Matter*, 7(23):4433, 1995.
- [4] Douglas J. Paul. *Efficiency vs. temperature of materials with different ZT*, 2009.
- [5] Yawei Shen, Chao Li, Rong Huang, Ruoming Tian, Yang Ye, Lin Pan, Kunihiro Koumoto, Ruizhi Zhang, Chunlei Wan, and Yifeng Wang. Eco-friendly p-type Cu_2Sns_3 thermoelectric material: crystal structure and transport properties. *Scientific reports*, 6:32501, 2016.
- [6] Alex M Wiltrout, Carlos G Read, Evan M Spencer, and Raymond E Schaak. Solution synthesis of thiospinel CuCo_2S_4 nanoparticles. *Inorganic chemistry*, 55(1):221–226, 2015.
- [7] Chong Xiao, Jie Xu, Kun Li, Jun Feng, Jinlong Yang, and Yi Xie. Superionic phase transition in silver chalcogenide nanocrystals realizing optimized thermoelectric performance. *Journal of the American Chemical Society*, 134(9):4287–4293, 2012.
- [8] Ying-Teng Zhai, Shiyong Chen, Ji-Hui Yang, Hong-Jun Xiang, Xin-Gao Gong, Aron Walsh, Joongoo Kang, and Su-Huai Wei. Structural diversity and electronic properties of $\text{Cu}_2\text{Sn}_x\text{S}_3$ ($x = \text{s, se}$): A first-principles investigation. *Physical Review B*, 84(7):075213, 2011.

- [9] Xiao Zhang and Li-Dong Zhao. Thermoelectric materials: Energy conversion between heat and electricity. *Journal of Materiomics*, 1(2):92–105, 2015.
- [10] Huiwen Zhao, Xiaoxuan Xu, Chao Li, Ruoming Tian, Ruizhi Zhang, Rong Huang, Yinong Lyu, Dongxu Li, Xiaohui Hu, Lin Pan, et al. Cobalt-doping in Cu_2Sns_3 : Enhanced thermoelectric performance by synergy of phase transition and band structure modification. *Journal of Materials Chemistry A*, 5(44):23267–23275, 2017.
- [11] Lanling Zhao, Xiaolin Wang, Frank Yun Fei, Jiyang Wang, Zhenxiang Cheng, Shixue Dou, Jun Wang, and G Jeffrey Snyder. High thermoelectric and mechanical performance in highly dense Cu_{2-x}S bulks prepared by a melt-solidification technique. *Journal of Materials Chemistry A*, 3(18):9432–9437, 2015.